Mass Transport Deposits and geo-hazard assessment in the Bradano Foredeep (Southern Apennines, Ionian Sea)

Marine Geology xxx (2018) xxx-xxx

Contents lists available at ScienceDirect

Marine Geology

journal homepage: www.elsevier.com

Mass Transport Deposits and geo-hazard assessment in the Bradano Foredeep (Southern Apennines, Ionian Sea)

Andrea Artoni[a, *], Alina Polonia[b], Mirko Carlini[a], Luigi Torelli[a], Paola Mussoni[a, c], Luca Gasperini[b]

[a] Department of Chemistry, Life Sciences and Environmental Sustainability, University of Parma, Parco Area delle Scienze, 157/A, Parma, Italy
[b] Institute of Marine Science CNR ISMAR-Bo, Via Gobetti, 101, 40129 Bologna, Italy
[c] ENI S.p.A., E & P Div., Via Emilia, 1, 20097 San Donato Milanese, MI, Italy

ARTICLE INFO

Editor: Michele Rebesco

Keywords:
Southern Apennines
Foredeep basin
Mass Transport Deposits
Quantitative mapping
Geo-hazards

ABSTRACT

Seafloor bathymetry, combined with multi-scale seismic reflection profiles, were used to describe the morphostructural setting of the Bradano Foredeep (Gulf of Taranto, northern Ionian Sea), where a submerged portion of the Southern Apennines is facing the Apulia Platform in the Calabrian Arc convergent margin. In this complex area, marine geophysical data highlight the presence of two mega-slide deposits at the shelf-slope transition, which are most likely the largest ever described in the region. These slid masses, named the Bradano Basento MegaSlide (BBMS) and Bradano Basento MegaSlide 1 (BBMS1), form a Mass Transport Deposit Complex (MTDC) affecting and eroding the topmost portion of the outer Apennines deformation front and the Apulian Foreland Ramp. It was emplaced in late Pleistocene times inside the narrow (about 10 km wide) Bradano Foredeep basin, a Plio-Pleistocene submarine trough developing at the chain front. The youngest of these deposits (BBMS1) likely predates the Last Glacial Maximum. Location of the MTDC within the subduction complex suggests that active tectonics and seismic shaking might represent the main triggering mechanisms for gravitative instability in this area, although gravitational tectonics and sediment creeping mechanisms cannot be excluded. On the other hand, size and distribution of the MTDC in the sedimentary record of the Bradano Foredeep suggest the need of re-evaluating the potential for large earthquakes/tsunamis, and more in general geological hazard related to submarine sliding masses, along the coast of this highly populated area.

1. Introduction

Along convergent margins, mass-transport represents an important mechanism for sediment distribution within sedimentary basins. This process can be triggered or favored by several causes, including: seismic shaking (Satake, 2012; Strasser et al., 2013); sea-level changes (Maslin et al., 1998; Rothwell et al., 1998); gas hydrate dissociation (Maslin et al., 1998; Brown et al., 2006); volcanic activity (Urgeles et al., 1999); changes in pore-pressure (Grall et al., 2014); and asperities (e.g. sea-mount) of the subducting plate that interacts with the overriding plate (Ruh, 2016). In such settings, sediment transfer is occasionally sudden and, especially if related to seismic activity, mass failure can generate tsunamis (Von Huene et al., 2004; Lo Iacono et al., 2012; Kawamura et al., 2014). The destructive potential of these events is proportional to the volume, vertical displacement, water depth and speed of the mobilized masses (Álvarez-Gómez et al., 2011; Lo Iacono et al., 2012; McAdoo and Watts, 2004; Murty, 2003; Schnyder et al., 2016). Relatively small bodies can cause tsunami waves as high as tens of meters (Bohannon and Gardner, 2004; Von Huene et al., 2004).

Because of their geo-hazard potential, Mass Transport Deposits (MTDs) have received greater attention, and have been extensively recognized and investigated in the historical and geological records (Zitter et al., 2012; Festa et al., 2014; Martín-Merino et al., 2014). MTD units are characterized by chaotic acoustic facies, and their emplacements may strongly modify the seafloor morphology (Rebesco et al., 2009; Yamada et al., 2012; Katz et al., 2015; Eruteya et al., 2016). Although MTDs are easily recognized in high resolution seismic images, detailed mapping allowing for volume evaluation of the transported material is still lacking in many regions (Craig Shipp et al., 2011; Yamada et al., 2012; Moscardelli and Wood, 2015), including the Gulf of Taranto. Mass movements of different sizes and ages have been identified through geophysical investigation in the Bradano Foredeep (Rebesco et

* Corresponding author.
Email address: andrea.artoni@unipr.it (A. Artoni)

https://doi.org/10.1016/j.margeo.2018.11.008
Received 12 September 2017; Received in revised form 31 October 2018; Accepted 11 November 2018
Available online xxx
0025-3227/

al., 2009; Ceramicola et al., 2014; Meo et al., 2016) but without a detailed quantitative analysis of geometry, origin and triggering mechanism. In this work, we describe two large Mass Transport Deposits in the Bradano Foredeep that were large enough to have potential for generating destructive tsunamis. Mapping of the deposits by seismic reflection techniques and borehole data provides the dimensions, evidences for recognizing their thixotropic properties and useful constraints to modelling possible tsunami wave/s generated by the MTD in the Gulf of Taranto. These data are used to assess the geohazard associated with such mass failures in the region surrounding the Gulf of Taranto and the Central Mediterranean.

2. Regional setting

The Gulf of Taranto is site of pervasive tectonic deformation as part of a complex orogenic system that includes the Calabrian Arc, the Calabrian Accretionary Wedge, the Southern Apennines and the Apulian Foreland Ramp (Fig. 1). The Calabrian Arc is a tight arcuate orogen connecting the Southern Apennines with the Maghrebian chain in Sicily (Gueguen et al., 1998; Bonardi et al., 2001; Rossetti et al., 2004) (Fig. 1a). It is characterized by an active front in the Ionian Abyssal Plain, segmented by across-strike transcurrent and trans-tensional fault zones (Bortoluzzi et al., 2017; del Ben et al., 2008; Polonia et al., 2011, 2016a, 2017b; Van Dijk et al., 2000). The Sangineto Line, one of these

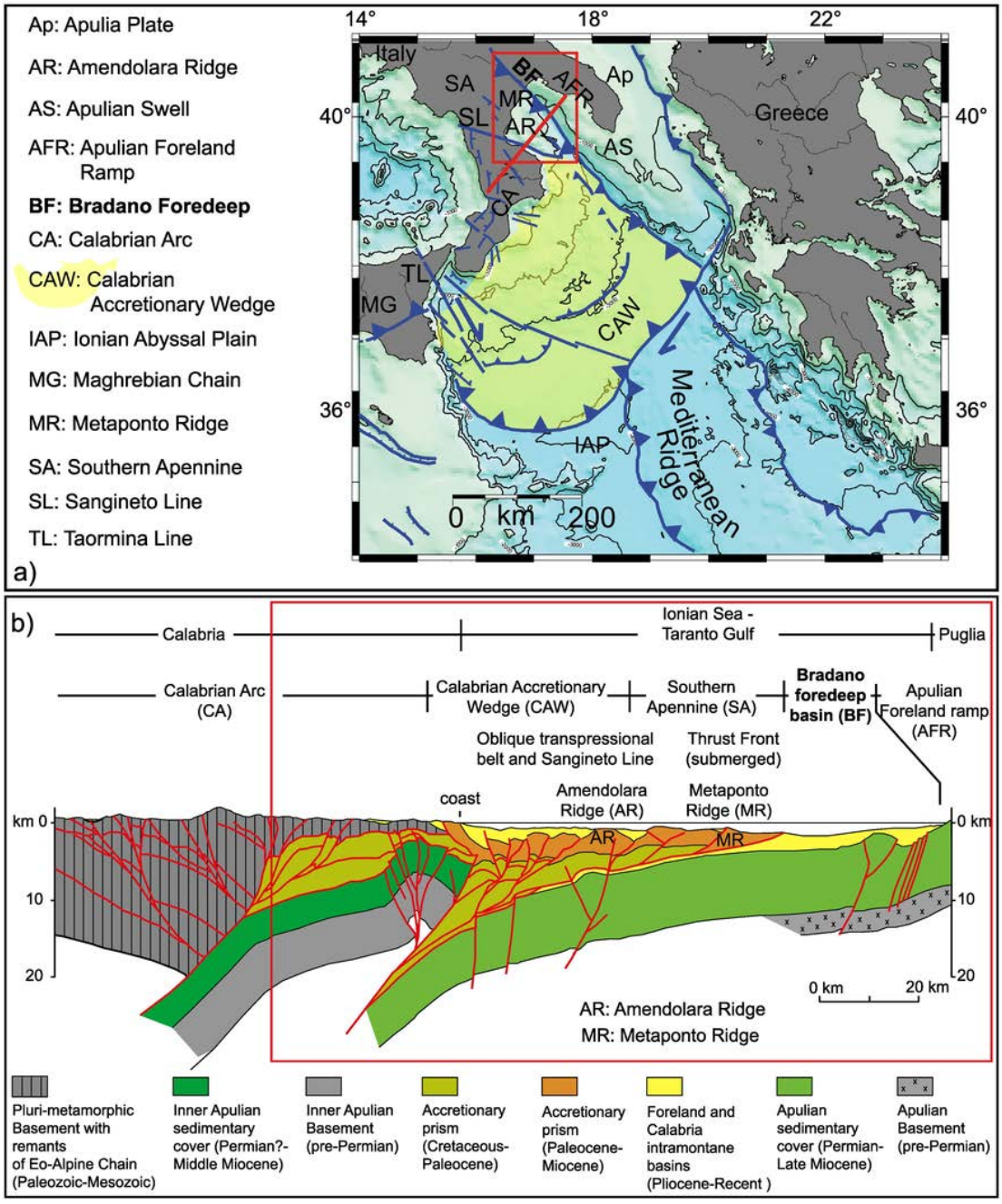

Fig. 1. The Gulf of Taranto in the Central Mediterranean region; a) working area (red box) and main geodynamic domains (SA = Southern Apennines; CAW = Calabrian Arc Accretionary Wedge; AP = Apula-Adria plate) modified after Van DijK et al. (2001). b) Regional cross section across the Gulf of Taranto from Calabrian Arc to Apulia Foreland ramp (after (Van Dijk et al., 2000). (For interpretation of the references to colour in this figure legend, the reader is referred to the web version of this article.)

fault zones, is a major ESE-WNW trending lithospheric structure that separates the Calabrian Arc from the Southern Apennines; it forms the oblique contractional belt of the Amendolara Ridge in the southern Gulf of Taranto (Bonardi et al., 2001; Ferranti et al., 2014; Van Dijk et al., 2000; Volpi et al., 2017) (Fig. 1a). North of the Sangineto Line, the Southern Apennines are made of eastward verging stacks of Mesozoic oceanic-derived units, overthrusting Mesozoic-Cenozoic carbonate platform sediments (Figs. 1a, b) and the basin units of the Apulia plate (Mostardini and Merlini, 1986). These latter comprise a 35 km-thick continental crust containing Paleozoic basement and a ~6 km thick Mesozoic carbonate sedimentary succession, that is unconformably overlain by a Paleogene to recent succession. This latter unit mainly consists of shallow-water deposits (Ricchetti et al., 1988; Doglioni et al., 1999).

The external fronts of the Calabrian Arc and the Southern Apennines progressively migrated toward the ESE above the subducting Apulia and Ionian lithospheres during the Neogene and Quaternary (Fig. 2) (Billi et al., 2011; Jolivet and Faccenna, 2000; Malinverno and Ryan, 1986; Reilinger and McClusky, 2011; Rossi et al., 1983). The fronts suffered a significant reorganization since the Messinian Salinity Crisis (Reitz and Seeber, 2012; Rouchy and Caruso, 2006; Roveri et al., 2014) (Fig. 2). The collisional setting was responsible for the formation of the Bradano Foredeep Basin starting from the Pliocene (Fig. 2) with the Apulian Foreland Ramp down-flexed toward the west (Doglioni et al., 1994). The Southern Apennines units moved eastward of about 40 km during the early-late Pliocene (~4 Ma) (Van Dijk et al., 2000; Butler, 2009) (Fig. 2). A major tectonic pulse (Pescatore and Senatore, 1986; Patacca and Scandone, 2004) was recognized coeval with an uplift of the Apulian swell (Doglioni et al., 1994) and underthrust of the foredeep basin below the Apennines in the early Pliocene (Figs. 1b, 2). Uplift and isostatic rebound processes prevailed after the early Pleistocene (Palano et al., 2012; Faccenna et al., 2014), as marked by recent shelf deposits sealing the outermost front of the subduction/collisional system. Recent geological and geophysical data outline that during the last 1 Ma (Middle Pleistocene, Fig. 2) the Calabrian Arc and the Southern Apennines were uplifted at a rate of up to 1 mm/y (Billi et al., 2011; Faccenna et al., 2014) and this uplift rate could have enhanced erosion, gravitational instability and sediment remobilization during seismic activity.

2.1. Seismicity

The Gulf of Taranto area has been tectonically active since the Pliocene (Doglioni et al., 1999; Catalano et al., 2001). However, deformation rates appear to have recently decreased in response to a plate boundary reorganization and the deactivation of the Apulia plate roll-back (Faccenna et al., 2014; Ferranti et al., 2014). Despite this deactivation should have resulted in a lower seismic activity, recent earthquakes are observed in this area (Fig. 3), and the historical earthquake catalogue shows rare (4–5 events) but significant large-magnitude events (maximum magnitude 6.18) between 1000/461 BCE and the present (Guidoboni et al., 2015; Locati et al., 2016). Few earthquakes aligned along major known structures occurred after the 1977 with Mw ≥ 3.5 whose focal plane solutions are representative of thrust, extensional and strike-slip events (DISS Working Group, 2015). Seismic epicenters are mainly located onshore, in the accretionary wedge and along the Southern Apennines front, with hypocenter depths generally shallower than 10 km, but reaching up to 400 km (Fig. 3). In the Apulian Foreland Ramp, seismic activity is more diffused and less well constrained due to the lack of seismometer stations in the marine region. No paleoseismological reconstructions are available to date for the Gulf of Taranto region, except for few studies dealing with onshore fault systems (Galli et al., 2008; Galli and Peronace, 2015). Despite the small magnitude diffuse seismicity, seismic hazard in the Gulf of Taranto is

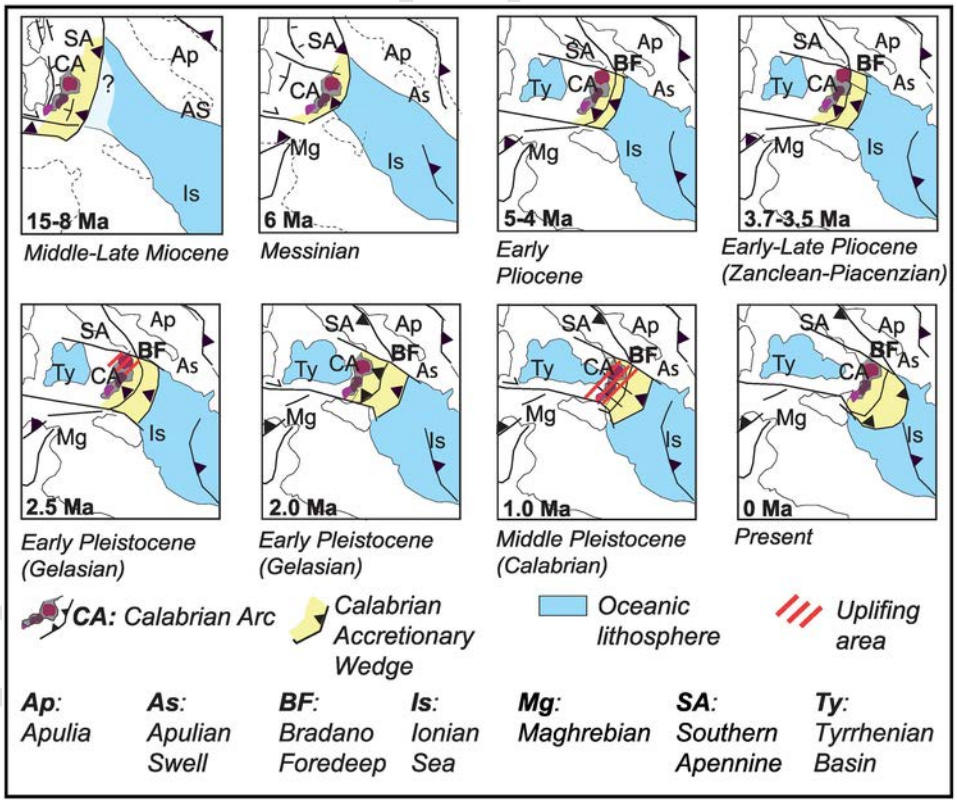

Fig. 2. Neogene tectonics of the Gulf of Taranto, in the frame of collision between Calabrian arc, Southern Apennine and Apulian Swell modified after (Capozzi et al., 2012; Zecchin et al., 2015). The evolutionary steps since middle-late Miocene to present are related to the tectono-sedimentary cycles in Fig. 5.

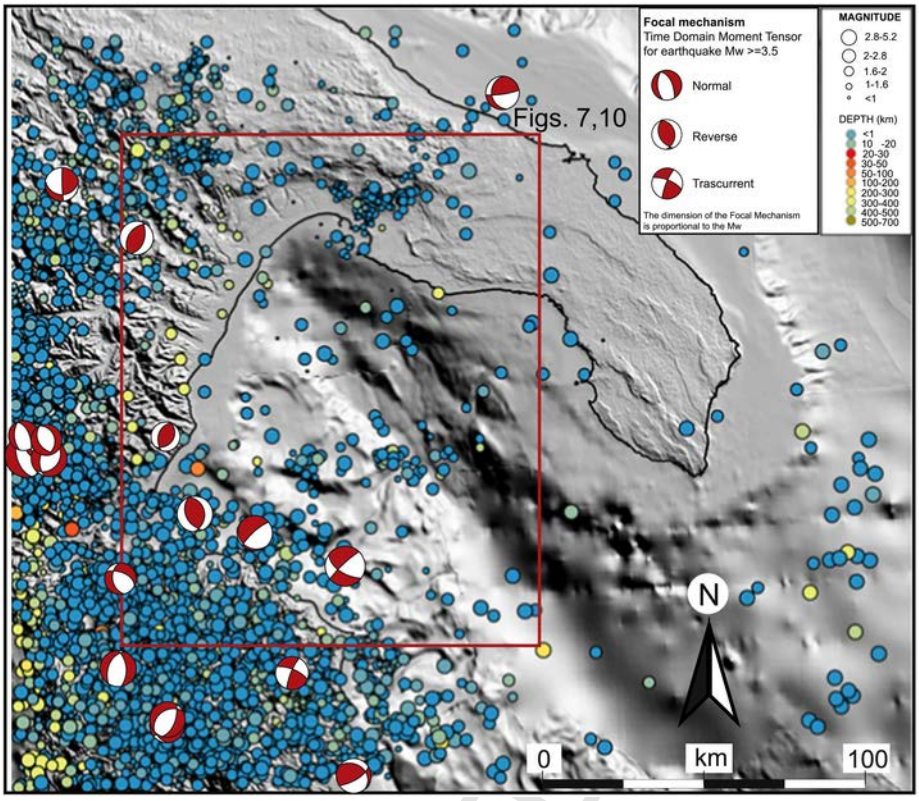

Fig. 3. Mw > 3 earthquake epicenters (1990–2016) from ISIDe Italian Seismological and Instrumental Data-basE AHEAD Working Group the European Archive of Historical Earthquake Data (DISS Working Group, 2015; ISIDe working Group, 2016; Locati et al., 2014). Main focal mechanisms calculated since 1977 are also included. Bathymetry is from EMODnet Digital Bathymetry (DTM) (http://portal.emodnet-bathymetry.eu/).

associated with expected maximum magnitude events reaching up to Mw 7 (Rovida et al., 2011), similarly to surrounding areas in the Calabrian Arc.

3. Data and methods

3.1. Morphobathymetry

Bathymetric data were derived from the Global Multi-Resolution Topography (GMRT) dataset, available at http://www.geomapapp.org and https://www.seadatanet.org/, which host high-resolution (~100 m in the deep sea) bathymetry from various databases (Table 1). Data were analyzed and displayed using the Global Mapper v. 16 software (http://www.bluemarblegeo.com/) and artwork software Adobe Illustrator CS5.

3.2. The subsurface dataset: exploration wells and seismic reflection profiles

A total of 25 exploration well-logs are available in the study area (Videpi database at http://unmig.sviluppoeconomico.gov.it/videpi/). The geological and geophysical logs available for the wells are reported in Table 1. Seven well-logs, listed in Fig. 4, were used to define a stratigraphic framework in the vicinity of the studied MTD and to correlate these data to the stratigraphic units described in the Gulf of Taranto (see Section 4.1; Figs. 5, 6). Analysis was carried out considering lithology, unconformity surfaces, faunal content and biozones provided by the composite well-logs (Fig. 6).

About 2000 km of commercial multichannel seismic profiles of the Italy offshore (zones D and F) were used to map and reconstruct the geometry of the studied MTD and to define the morpho-structural framework of study area (Fig. 7; Suppl. mat. 1). These seismic profiles, acquired for deep subsurface hydrocarbon exploration by ENI Spa between 1970 and 1990, are available at http://unmig.sviluppoeconomico.gov.it/videpi/ (Table 1). The commercial multichannel seismic reflection profiles of the Zone F dataset (Table 1) were migrated in time with Seismic Unix (Cohen and Stockwell, 2010; Stockwell, 1997, 1999) and interpreted with the aid of Kingdom Suite 2D/3Dpack Module (IHS Kingdom® - v. 8.15) together with seismic reflection profiles of the other datasets (Zone D dataset in Table 1) (Figs. 8, 9). Eight seismic reflection profiles were selected to map the MTD (Fig. 4) with the aid of the Move Software (Midland Valley™ v. 2017). The regional multichannel profile, Line-A of Zone D dataset (Fig. 9; Table 1), was selected as the most representative among the whole dataset, since it is close to the exploration wells (Fig. 4). It was depth-converted (Suppl. mat. 2) and used as a reference section for the depth-conversion of the other seismic reflection profiles. The depth-converted seismic reflection profiles were used to reconstruct the geometries, bounding surfaces and volume of MTD (see Section 5.2). Lithological changes and dip meter measurements in well logs as well as changes in the dips of the reflections were key data to define the detachment of the MTD (see Section 5.2.3).

3.3. 3-D modelling

Mapping of the MTD was carried out through different steps and after comparing among solutions of different interpolation methods of the software Move™ (Midland Valley v. 2017) (see Appendix 1). The 3-D modelling of the MTD extension and volume was performed after depth-conversion of seismic profiles (Suppl. mat. 2). The MTD was reconstructed on eight selected seismic profiles with different orientations. The seismic reflection profiles form a grid in between ~2 × 10 km and ~10 × 10 km (Fig. 7). In between the interpreted

Table 1
List of the dataset employed in this study.

Bathymetry and topography			
Source	Dataset available	Dataset used in this study	resolution
Shuttle Radar Topography Mission (SRTM) (https://earthexplorer.usgs.gov) or GMRT dataset available from http://www.geomapapp.org (Ryan et al., 2009)	1 Arc-Second void filled global elevation data	Land area (Figs. 3, 4, 7, 10)	30 m cell size
EMODnet Bathymetry Consortium (2016) http://portal.emodnet-bathymetry.eu/ http://doi.org/10.12770/c7b53704-999d-4721-b1a3-04ec60c87238 or GMRT dataset available from http://www.geomapapp.org (Ryan et al., 2009)	EMODnet Digital Bathymetry (DTM).	Marine area (Figs. 3, 4, 7, 10)	175 m cell size
Italian Navy Hydrographic Office http://seadatanet.maris2.nl/v_edmo/print.asp?n_code = 1338		Figs. 11, 12	100 m cell size

Exploration well		
Source	Dataset available	Dataset used in this study
Ministero dello sviluppo economico DGS-UNMIG (Direzione Generale per la Sicurezza anche Ambientale delle Attività Minerarie ed. Energetiche - Ufficio Nazionale Minerario per gli Idrocarburi e le Georisorse) http://unmig.sviluppoeconomico.gov.it/ViDEPI (Visibilità dei Dati afferenti all'attività di Esplorazione Petrolifera in Italia) http://unmig.sviluppoeconomico.gov.it/videpi/	Well contains various logs: lithology log; cuttings log; stratigraphy. Well contains geophysical logs: spontaneous potential (SP); resistivity; dipmeter; sonic	11 well-logs listed in Figs. 6, 17

Seismic reflection profile			
Geophysical multi-scale dataset	Acquisition parameters	Main processing sequence	Vertical resolution
Zone F dataset	Acquisition date: 1975 Source: Vaporchoc (depth 6 m) Streamer: 2400 m (depth 18 m) Groups 48 group interval: 50 m Field recorder SN 338 filter 1/8–125 floating point_sampling 4 msec Geophones type HC 201 n°48/group Coverage: 48fold Sampling rate: 4 msec	Amplitude recovery WAPCO (stabilization by vaporchoc signal) Muting Deconvolution 240 ms windows 500–2300 msec (below seabottom) 1900–3600 msec (below seabottom) Velocity analysis NMO (linear interpolation between functions) Stack 4800% Time variant filter (origin sea bottom)	≈7–15 m in the first 2 s velocity 1600–2200 m/s

Table 1 (*Continued*)

Seismic reflection profile			
Geophysical multi-scale dataset	Acquisition parameters	Main processing sequence	Vertical resolution
Zone D dataset	Acquisition date: 1968 Source: air gun (average seis depth 11 m) Cable: 1600 m Group interval: 65 m Shot point interval 4 × 33 m Average shot offset 397 m Record length 5 Sampling: 4 msec	Seis edit NMO Deconvolution 240 ms windows 500–2300 msec (below seabottom) 1900–3600 msec (below seabottom) Stack 24-fold	≈9–15 m in the first 2 s velocity 1600–2200 m/s

seismic profiles, the software generated the modelled surfaces based on sample density of additional 100 lines and resampling along line at an interval between 30 m and 1000 m forming a modelling grid of ~30 × 30 m or ~1000 × 1000 m over an area of 28 × 26 km (Fig. 18). Appendix 1 shows details of data interpolation and modelling.

4. Stratigraphic and structural setting of Gulf of Taranto

4.1. Stratigraphy

Based on published data (Fig. 5) and data used in this study (Fig. 4), the main stratigraphic framework of the Taranto Gulf in the surrounding of the studied MTDs is defined for the Messinian to Holocene. The Messinian Salinity Crisis deposits are represented by primary and resedimented evaporites accreted within the accretionary prism and by discontinuous, few tens of meter thick and shallow water limestone and marly sediments deposited on the Apulian Foreland Ramp (Fig. 6). In both tectonic settings, regional major unconformities bound the Messinian deposits (Bonardi et al., 2001; Roveri et al., 2014; Zecchin et al., 2013). The topmost section of the Gulf of Taranto sedimentary sequence is made of Pliocene to present-day shallowing-upward deposits (Pescatore and Senatore, 1986; Zecchin et al., 2015). The sequence starts with deep-water, fine-grained turbidite layers, passing to continental shelf, deltaic, coastal and alluvial deposits (Pescatore and Senatore, 1986; Zecchin et al., 2015).

East of the Metaponto Ridge, the Bradano foredeep is a Pliocene-Holocene subsiding basin filled by fine-grained deep-water turbidites and shelf deposits onlapping the Apulian Foreland Ramp (Figs. 8, 9). Neogene tectonics, coupled with eustatic sea level changes, were the main controls on sedimentation feeding the wedge-top basins of the Southern Apennines fold and thrust belt, the Bradano foredeep and the Apulia Foreland Ramp. The Pliocene-Pleistocene sequences have been described and correlated onshore (Patacca and Scandone, 2004; Zecchin et al., 2004, 2009; Tropeano et al., 2013; Amorosi et al., 2014) and offshore (Pescatore and Senatore, 1986; Zecchin et al., 2015). Four tectono-sedimentary cycles (P1–P4) are bounded by three major regional unconformities (MPCU, EPSU, MPSU from older to younger, Fig. 5) that are related to main tectonic pulses of the Calabrian Accretionary Wedge and of the Southern Apennines (Fig. 2) (Zecchin et al., 2015) and observable also in the study region (Fig. 6). The four first-order sedimentary cycles show higher frequency variations mainly related to the interplay between regional uplift and eustacy (Zecchin et al., 2011, 2016). The transgressive post Last Glacial Maximum (LGM) deposits, starting from ~20,000 years BP (Lambeck et al., 2014) preserve the transition from alluvial to deltaic, then shelfal and finally to basin plain environments prograding southward during the Holocene.

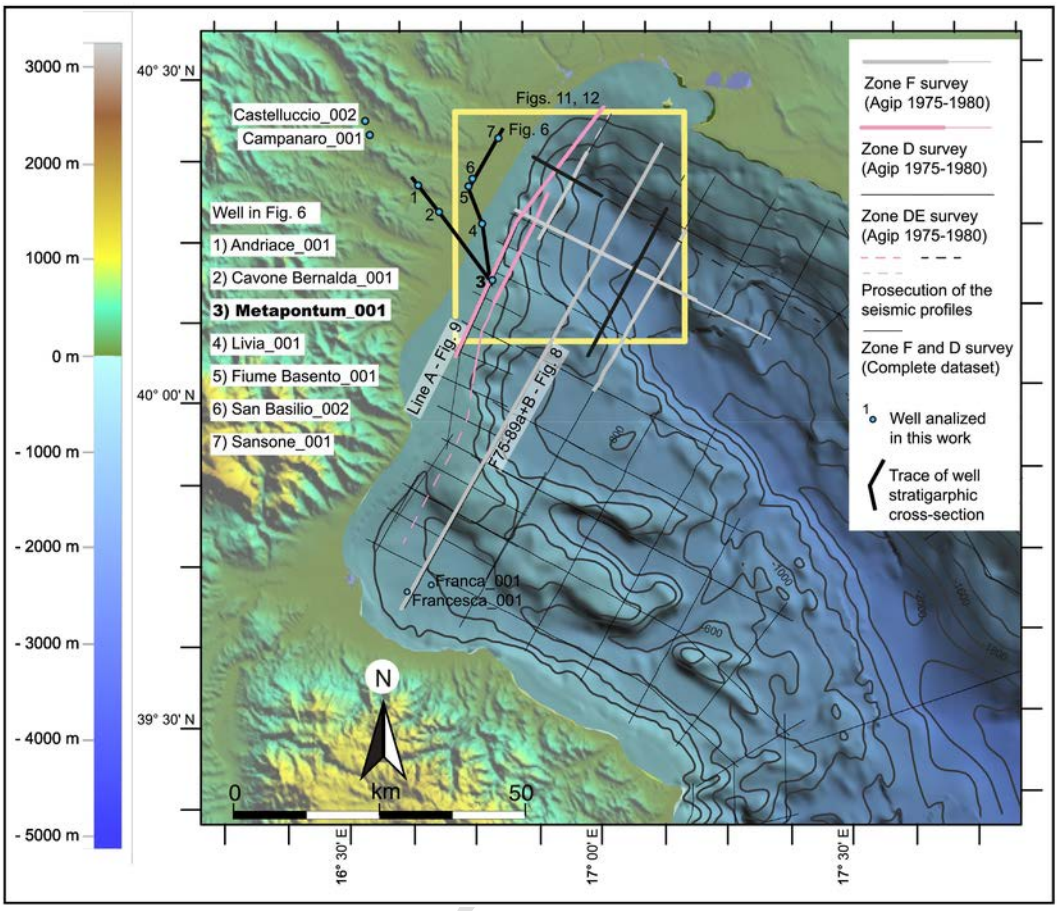

Fig. 4. Dataset employed over a shaded relief map of bathymetry and topography (GMRT dataset available from http://www.geomapapp.org (Ryan et al., 2009) (see Table 1). Locations of well logs used for stratigraphic correlations (Fig. 6) and seismic reflection profiles (Figs. 8, 9, 13–15; Suppl. mat. 1). Thin black traces are the position of seismic reflection profiles of Zone F and D surveys. Thicker coloured traces are the position of selected seismic reflection profiles in Figs. 8, 9, 13–15 and Suppl. mat. 1.

This sequence is up to 100 m thick (Caputo et al., 2010; Tropeano et al., 2013; Zecchin et al., 2015, 2016) onland and in shelfal area (Fig. 6).

4.2. Structural setting

Re-interpretation of seismic reflection profiles integrated with published structural maps (Bigi et al., 1990; Carbone et al., 2013; Ferranti et al., 2014; Rossi et al., 1989; Teofilo et al., 2018) image main tectonic features in the study area (Figs. 7–9 and Suppl. mat. 1).

The northern portion of the Gulf of Taranto contains the oblique contractional belt of the Amendolara Ridge and the submerged Southern Apennines fold and thrust belt, represented by the Metaponto Ridge (Fig. 1b). This NW-SE oriented structural high corresponds to the western flank of the Bradano Foredeep and represents the outermost thrust front of the Southern Apennines (Figs. 7–9). The latter merges toward the south with the southern termination of the Amendolara Ridge (Fig. 7). The Metaponto Ridge is made of imbricated thrust sheets, which generate thrust-related folds with complex hinges and hinge-related extensional faults in form of minor localized deformations (Figs. 8–9; Suppl. mat. 1). Exploration wells show that the frontal thrust of the Metaponto Ridge is actually made of two stacked thrust sheets made of Mesozoic-Cenozoic allochthonous units (Figs. 6, 8, 9; Suppl. mat. 1). The deeper of these tectonic units lays on the roof of the subducting Apulia Plate (Figs. 8, 9). It detaches at the top of the Messinian/early Pliocene deposits and is made of Pliocene accreted deposits (A_P3/2 in Figs. 8-9). The shallower thrust sheet brings Cretaceous to late Miocene sedimentary units above middle-late Pliocene foredeep deposits (Figs. 6, 8, 9; Suppl. mat. 1). Late Pliocene-Pleistocene gently folded deposits seal the Metaponto Ridge Frontal Thrust (Figs. 8, 9).

East of the Taranto Valley, the Apulian Foreland Ramp plunges underneath the submerged Bradano Foredeep basin and below the southern termination of the Southern Apennines front (Figs. 8–9; Suppl. mat. 1). Combined analysis of seismic reflection profiles and well-logs show that thrust and thrust-related anticlines affect the whole Apulian Foreland Ramp, even underneath the Apennines (Figs. 8–9 and Suppl. mat. 1). These deep thrusts form very open anticlines accommodating incipient collision expressed by NW-SE and N-S striking thrust-related folds (Fig. 7).

Inside the Pleistocene deposits of the Bradano Foredeep, the re-interpreted seismic reflection profiles image a lens shape body that affects the sea-floor morphology and shows internal geometries that change from shelf to basin plain (from NW to SE; Figs, 8, 9 and Suppl. mat. 1). This body results to be a Mass Transport Complex described in the following chapters.

5. Results

5.1. Seafloor morphology

The tectonic structures described above (Section 4.2) control the complexity of seafloor morphology in the area, characterized by scarps, drainage patterns and sedimentary basins, resulting from the interplay between deep faults, shallow deformations and sedimentary processes (Figs. 7, 10). Analysis of morphobathymetric data suggests the ex-

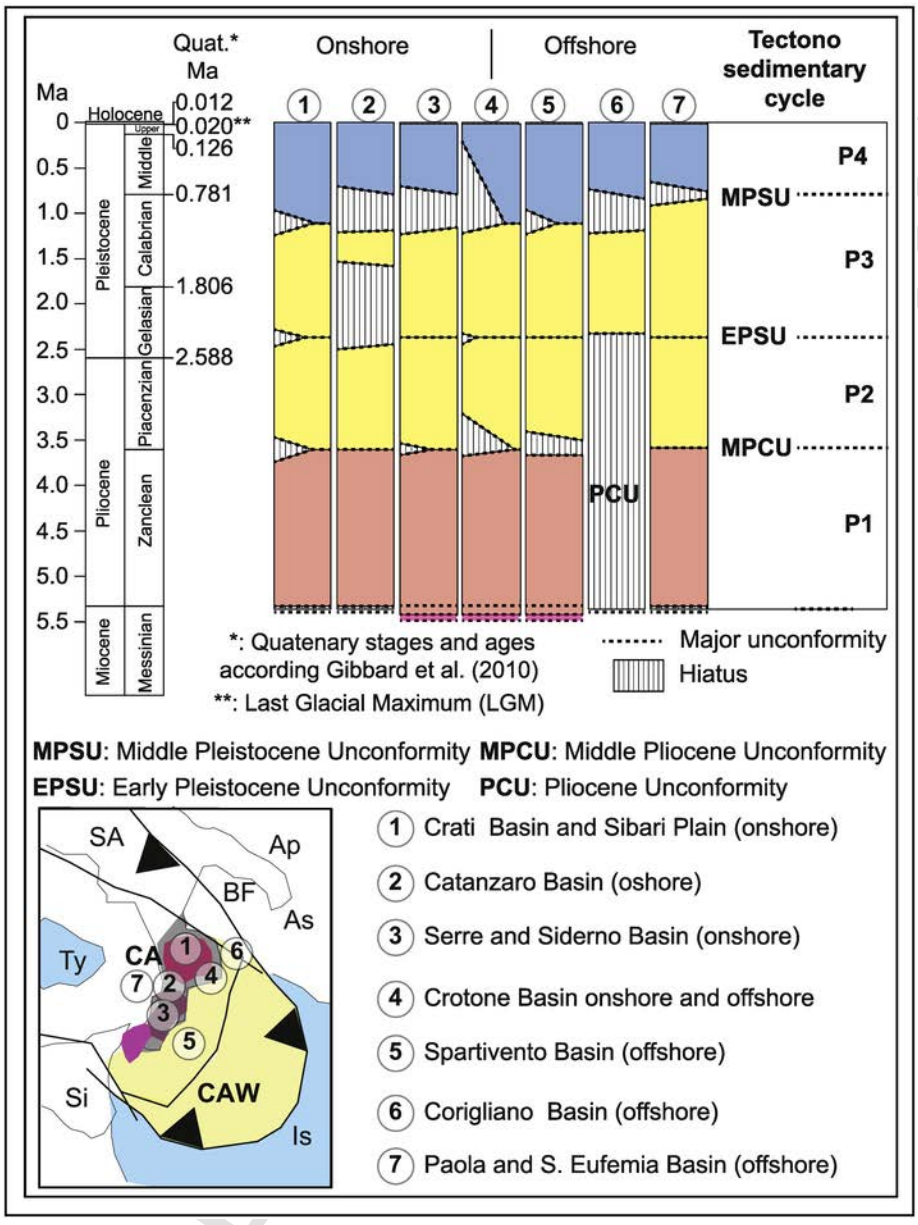

Fig. 5. Stratigraphic synthetic logs of the tectono-sedimentary cycles of the Calabrian Arc and Calabrian Accretionary Wedge according to (Zecchin et al., 2015) in selected area (1 to 7 in the inset at the bottom left corner - labels as in Fig. 1a). Quaternary stages and ages (Quat.*) according to (Gibbard et al., 2010).

istence of three morpho-structural domains, all affected by mass-wasting processes (Fig. 10): 1) the *western domain*, west of the Taranto Valley, characterized by the presence of ridges, valleys and intervening intra-slope basins; 2) the *central depression*, i.e., the Taranto valley; and 3) the *eastern domain*, east of the Taranto Valley, made of a wide westward-dipping shelf and slope with smooth morphologies.

The western domain belongs to the Ionian-Calabrian margin and is part of the submerged Southern Apennines chain. It is characterized by a relatively wide shelf (~11 km) delimited by the Sinni River, to the north, and the Ferro Stream, to the south (Fig. 10). North and south of this area, the shelf is very narrow (~2–3 km) (Fig. 10). The ridges and intervening intra-slope basins (e.g. Sinni and Sibari basins) are the morphologic expressions of interactions between the Apennine belt and the Calabrian accretionary wedge (Fig. 10). The Taranto Valley is about 317 km long and up to 10 km wide, and connects the Bradano and Basento alluvial plains (NNW), to the deep abyssal plain (Fig. 10), reaching depths of about 2200 m below sea level (m b.s.l.). The valley shows a western 15–30° steep flank and a relatively gentler eastern flank (~5–10°). The drainage network includes the Bradano submarine valley to the NW and two major canyons from the eastern domain, the Gallipoli and the Torre dell'Ovo canyons (Fig. 10). The head of the Bradano submarine valley is aligned with the mouth of the onshore Bradano River and they appear to cut and erode the shelf (Fig. 10). Similarly, Basento, Agri, and Cavone rivers incise the shelf and merge into the Taranto Valley (Fig. 10).

The NW-SE elongated eastern domain coincides with the western part of the down-flexing Apulia Peninsula, gently dipping to the SW. It is characterized by a ~3–30 km wide shelf that passes to a ~15–35 km wide continental slope incised by the Torre dell'Ovo and Gallipoli canyons. The steeper region (darker shades) at the base of the slope forms the eastern flank of the Taranto Valley (Fig. 10).

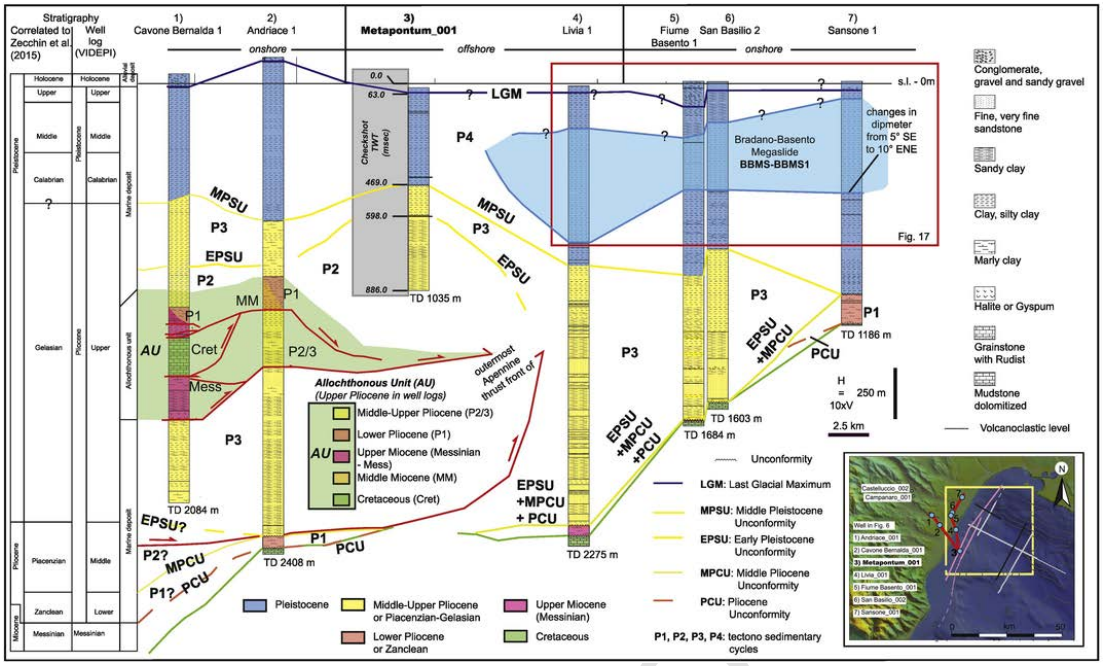

Fig. 6. Stratigraphic correlation of selected well-logs (for their location see inset map and Fig. 4). Metaponto 1 was used to depth-convert seismic profile Line-A (see Suppl. mat. 2). The stratigraphic units, the tectonic-sedimentary cycles (P1–P4) and the unconformities (MPCU, EPSU, MPSU) are as in Fig. 5; LGM is based on the appearance of coarse-grained alluvial deposits and the thickness of post-LGM deposits in onshore studies (Caputo et al., 2010; Tropeano et al., 2013; Zecchin et al., 2016).

5.2. Geophysical and geological evidences of slope instability processes

At the head of the Taranto submarine valley, at the confluence between the Bradano, Basento, Cavone and Agri submarine valleys (yellow square in Fig. 10), the seafloor morphology shows peculiar characters which cannot be assigned to any of the three morpho-structural domains defined above (Section 5.1). Short wavelength ridges and intra-slope basins shape the upper continental slope where the mouths of the rivers merge into the Taranto valley through a complex network of submarine valleys (Fig. 11). Marine geophysical data show that this area hosts a chaotic deposit never described before extending across a wide area including the Bradano/Basento submarine valleys and the Metaponto Ridge (Figs. 11, 12). Its geometry and internal structure can be considered the stack of two distinct mass transport events that we name Bradano Basento MegaSlide (BBMS) and Bradano Basento MegaSlide1 (BBMS1). Well-log correlation shows that the BBMS remobilizes middle-late Pleistocene, fine-grained (clay, silty clay) terrigenous deposits of Unit P4 (Fig. 6; see also Section 5.2.3).

5.2.1. The Bradano Basento MegaSlide (BBMS)

Bathymetric data and seismic images show that at the toe of the accretionary complex at the Metaponto Ridge, a uneven seabed morphology (Figs. 11, 12) is present above a lenticular body characterized by a chaotic, transparent and discontinuous seismic facies and delimited at depth by a high amplitude seismic reflection (Figs. 13–16). The SW flank of the BBMS is bounded by extensional faults striking sub-parallel to the Metaponto Ridge and dipping toward the NE (Fig. 12). Seismic reflection profiles Line-A and Line-B show locally some evidence of disrupted, chaotic and transparent reflections within the BBMS (Fig. 13a). The resolution of the seismic reflection profiles and the strong reflection at the seabed-water interface hamper the possibility to clearly identify the BBMS top surface that has been placed at the seafloor in most profiles (Figs. 13–16). However, some seismic profiles and well data suggest that sediments of variable thickness drape the BBMS (Figs. 14, 17). Despite these uncertainties, the top of the BBMS, as well as the likely sediment drape above it, appears undulated by open folds (Fig. 13). Within the BBMS, two main anticline hinges are visible on the seismic lines (hinges 1 and 2 blue in Fig. 13) and other hinges are observed at the seafloor (hinges 3, 4, 5 blue in Fig. 11). The limbs of these folds have steepness that generally increases toward the WSW and toward the NW (Fig. 11b and bathymetric profile A). These open folds are symmetric anticlines and strike E-W. To the SE, other symmetric anticlines show hinges that strike E-W (hinges 3, 4, 5 blue in Fig. 11) and are associated with extensional faults affecting the Metaponto Ridge (Figs. 11, 12). Because both extensional and contractional structures are observed, we suggest that the extensional faults are side-wall scarps, while the anticlines represent lateral compressional ridges of the BBMS. East and south of the Metaponto Ridge, the BBMS pinches out, its width tends to decrease to the S (Fig. 14) and it is cut by a second chaotic body named BBMS1 (see Section 5.2.2). The central portion of the BBMS shows plane-parallel reflections up to its flat top which is characterized by very low slope gradients (Fig. 11); faint wavy reflections are present and they likely are minor chaotic deposits (Fig. 16c). The disrupted seismic reflections belonging to theBBMS are bounded at depth by the basal gliding surface (Fig. 16) that is located within the clay-rich deposits of unit P4 (Fig. 17 and Section 5.2.3).

The BBMS forms a lens 31 by 19.5 km wide, corresponding to an area of 396 km^2 (Fig. 18a). Assuming that the average thickness of the likely draping sediments is about 50 m, the depth-conversion of seismic reflection profiles provides a maximum thickness for the BBMS of about ~600 m (0.5–0.7 s TWT) (see also Suppl. mat. 2) within an error of 7–15 m (Table 1), implying that the total volume of the sliding mass is about 132 km^3.

5.2.2. The Bradano Basento MegaSlide 1 (BBMS1)

Seismic data combined with seafloor morphology suggest that the overall chaotic body can be better described as a large-scale MTD formed by two distinct resedimented units, which show different deformation patterns, ramps and gliding surfaces.

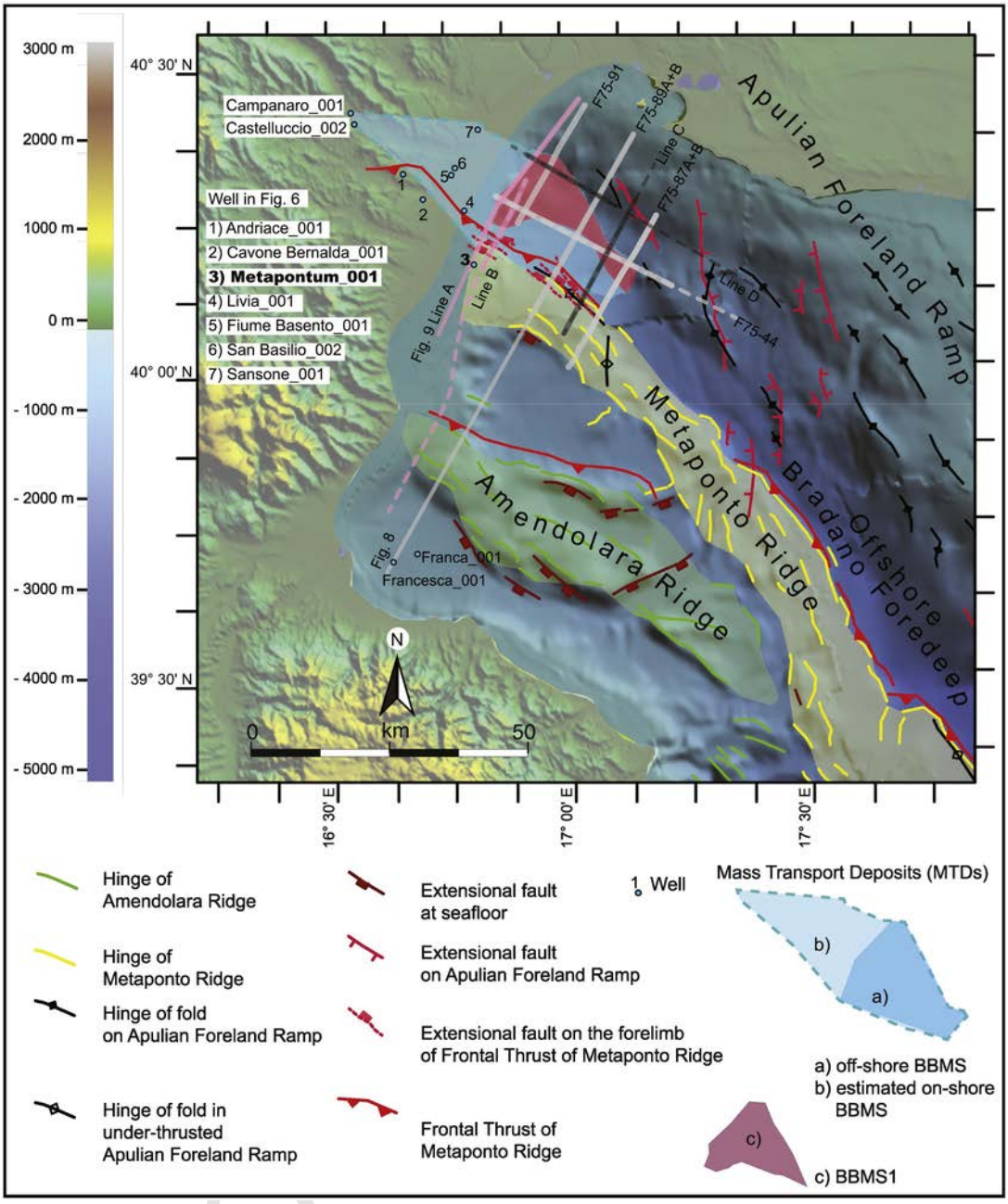

Fig. 7. Morpho-structural map of the Gulf of Taranto. Bathymetry is from different sources (see Table 1). Location of key seismic profiles that show the main tectonic structures of the area and used to map the MTDs (see Figs. 8, 9 and Suppl. mat. 1).

The NE flank of the MTD in the deepest foredeep basin is characterized by a lumpy/knobby morphology and a chaotic seismic facies while moving toward the SE, the MTD shows subtle and gentle folds with larger wavelengths (Figs. 13, 14). The deepest, more chaotic and deformed portion of the MTD body is interpreted as a distinct event of sediment remobilization (BBMS1) containing more chaotic and disrupted seismic reflections. As for the BBMS, the top surface of the BBMS1 is assumed to be the seafloor reflector, even though we cannot exclude that the chaotic body is covered by more recent sediments. The deformed layers of BBMS1 form WNW-ESE striking folds that vary from open to tight and locally verge toward the SSW (hinges 1 to 8 red in Figs. 11, 13). These folds have variable amplitudes (between 50 and 150 m) and wavelengths (between ~1 and ~2 km); slope gradients ranging from 3°–6° to 9°–12° (Fig. 11b). In the NW portion of the BBMS1, the folds are not associated with side-wall scarps, in contrast to what observed for the BBMS (Fig. 11). Instead, the headwall scarps visible on the Apulian margin are interpreted as related to the BBMS1 sliding processes that might have occurred toward SSW in agreement with the vergence of the folds (Figs. 11, 12). These folds can be described as compressional ridges perpendicular to the movement direction of the MTD.

The fold hinges 1 and 2 in red can be traced along the whole BBMS1 forming an arcuate belt that bounds the northeastern flank of the BBMS1 (Fig. 11). At the southeastern termination of the BBMS1, these folds become more gentle suggesting that fold amplitudes decrease from the NW to the SE where very open folds form a 1 km wide NW-SE striking compressional ridge (Figs. 13–15). To the SE, close to the lateral portion of the MTD, contractional features and extensional

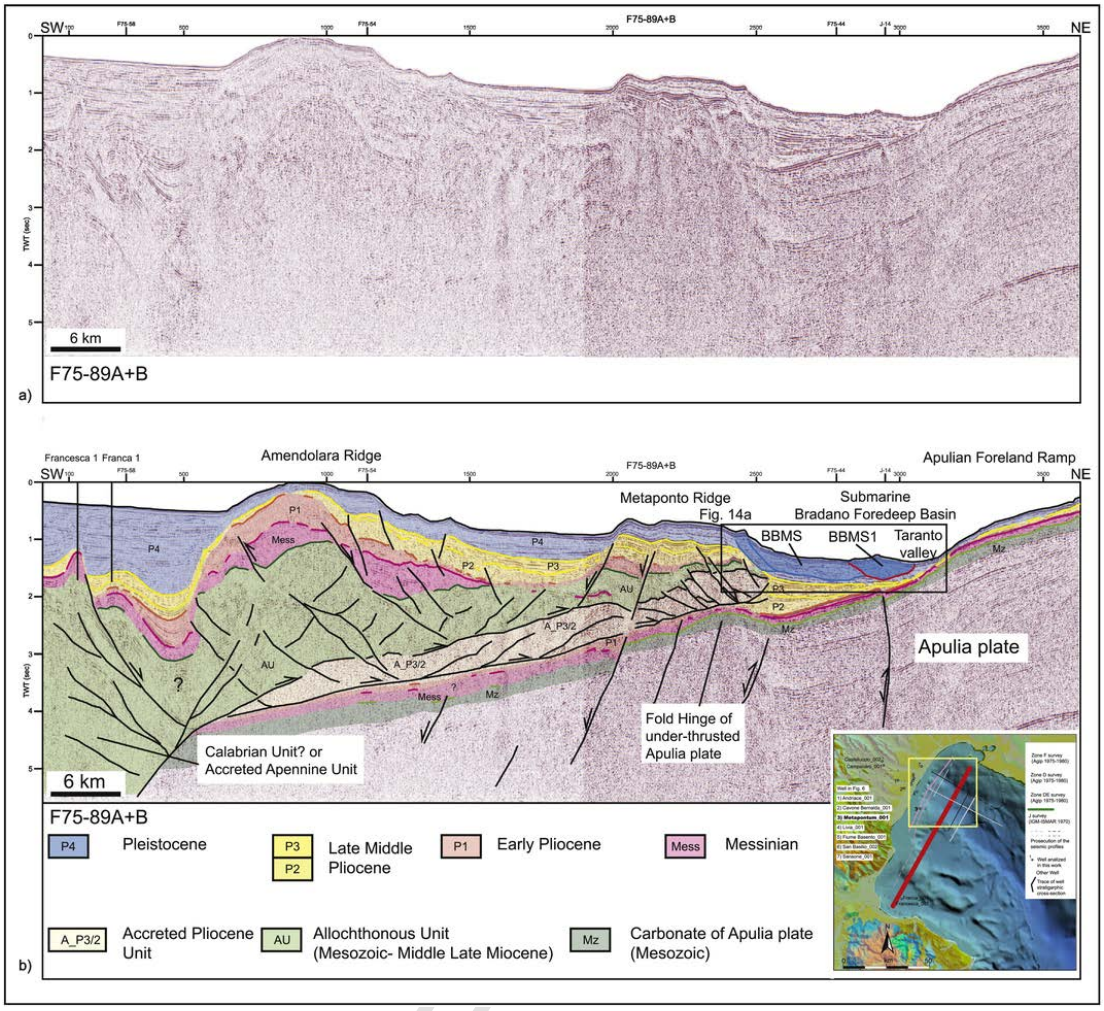

Fig. 8. Regional cross section F75-89A + B calibrated with well logs; a) original data; b) interpretation of the seismic reflection profile (see Suppl. mat. 1). The line F75-89A + B crosses the Amendolara and Meatponto Ridges. The Metaponto Ridge is made of two thrust sheets and it bounds the Offshore Bradano Foredeep and the undersea Taranto Valley (Figs. 10, 11). (For location see inset and Fig. 4.)

faults coexist and form minor scarps at the seafloor with few meters of throw (Fig. 15b).

The BBMS1 basal detachment coincides with that of the BBMS in the external region (Figs. 13–15) while, moving toward SW, it cuts through a ramp within the chaotic sediment assemblage and it bounds the more deformed portion of the BBMS1 from the less deformed BBMS (Figs. 13–16). In map view, the BBMS1 has a triangular shape, narrowing toward the SE where it shows a less pronounced seafloor roughness (Figs. 11, 12). In cross-section, the lenticular BBMS1 is 12 km long and 17.5 km wide for a total area of 153 km^2 (Fig. 18b). Its thickness is variable reaching a maximum of 600 m providing a total volume of 40–50 km^3.

5.2.3. *Extent of the BBMS-BMMS1 and the basal detachment*

The extent of the MTDs as deduced from our analysis should be considered conservative because the headwall scarp/s were not detected and the sediments draping the MTDs cannot be constrained accurately; the full extent of the MTDs is thus underestimated. The headwall scarps on the Apulian Margin may represent the source zone of BBMS1 (Fig. 11) while scarps observed along the NE flank of the Metaponto Ridge (Fig. 12) are side-wall scarps for the BBMS implying that the main headwall scarps of the BBMS should be located to the north. Onshore wells located close the NW margin of the BBMS-BBMS1 (Fig. 17) are characterized by logs which show variations in the dip meter profile at a depth of about 500 m b.s.l. and this is associated with a lithological change. In Sansone 1 well, at about 500 m b.s.l., a sharp variation in sediment layering (from 5°–6° toward the S-SE to 10°–8° toward the E-NE) is present (Fig. 17): the shallower sediment package seems to be tilted toward the S-SW with respect to the deeper sediments that likely represent the original depositional setting. Sediment dip variations are associated to lithological changes evidenced by both lithological and geophysical well logs (spontaneous potential and resistivity logs) across a transition from sand-rich lithologies to clay-rich lithologies at about 500 m b.s.l. (Fig. 17). The integrated analysis of dipmeter data, lithology and petrophysical information suggests that the exploration wells cross the MTDs gliding surface which, onshore, can be placed at about 500 m b.s.l. (Fig. 17). The S-SW sediment tilting agrees well with both the SSW fold vergence of the BBMS1 and BBMS1 movement direction as reconstructed through analyses of seismic reflection data (see Section 5.2.2).

The MTDs gliding surface as revealed by seismic data is represented by the strong and high amplitude reflections at a depth ranging between 1000 m and 2250 m b.s.l. (i.e. 750 m and 1000 m below sea floor) separating the chaotic and folded sediments above from the relatively well layered and undeformed sediment packets below (Figs. 13–16). The detachment surface shows an overall regular, concave upward geometry in SW-NE oriented sections (Figs. 13–14) and has an overall dip of 2°–3° toward SE along the length of the glided masses

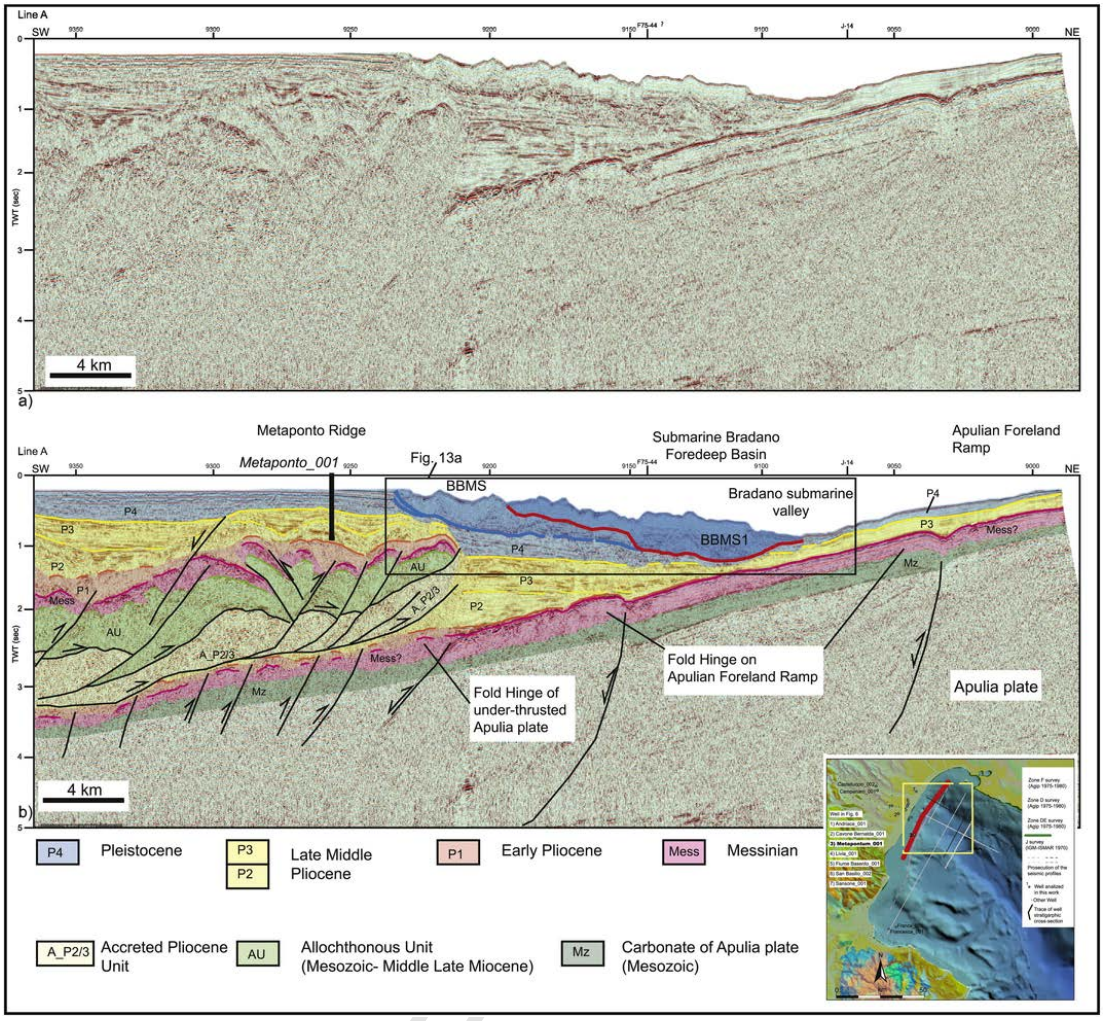

Fig. 9. a) Seismic reflection profile Line-A and b) its interpretation crossing the BBMS and BBMS1 where they are more deformed and chaotic inside (see Suppl. mat. 1 and Fig. 13a for details). This seismic reflection profile has been depth converted (see Suppl. mat. 2). (For location see the inset and Fig. 4.)

(Fig. 18d, e). Anomalies in the geometry of the basal detachment are observed in the NE border of the MTDs (Fig. 18d, e). These anomalies correspond to the few kilometers wide scours underneath the BBMS1 where truncations of the seismic reflections are visible (Figs. 13c, 14a and c, 15b). The rather regular geometry of the basal detachment differs from the more ragged geometry of the seafloor which is highly folded (Figs. 11, 12).

Since the MTD was sampled by onshore wells (Fig. 17), its NW boundary onland is placed where SE-dipping extensional faults displace middle Pleistocene marine terraces and may be associated with large scale instabilities (Bentivenga et al., 2004). In our reconstruction and considering the onshore extent, the BBMS-BBMS1 would be ~57 km long, and 22.5 km wide with a total area of 700 to 760 km^2 (depending on the filtering applied in the mesh construction, see Appendix 1) (Fig. 18c, f) and a total volume varying in between ~ 221 km^3 and 293 km^3 depending on the interpolation method that is applied. These dimensions would turn the BBMS into one of the largest MTD ever observed in the offshore Gulf of Taranto.

5.2.4. A mass-transport deposit complex (MTDC) of sliding masses

The integrated analysis of marine geophysical data and well logs suggests that the BBMS and BBMS1 headwall scarps are located to the NW (Figs. 11, 12), probably reaching onshore (Fig. 18). In the offshore region, the MTDs preserve their translational and accumulation zones. The translational zone is bounded by NW-SE striking side-wall scarps (Fig. 12) associated with lateral compressional ridges represented by open and long wavelengths anticlines suggesting that the BBMS has an overall movement toward the SE (Fig. 12): the mass moves parallel to the side-wall scarps and oblique to the lateral compressional ridges. The translation zone contains a portion of the BBMS that is mainly undeformed (Fig. 15): sediments preserve their original layering (plane-parallel reflections with internal faint wavy reflections) above a gliding surface (disrupted seismic reflections that mark the detachment surface). Such a slide mass suggests a mechanism of block sliding. The SE termination of the MTDs is the accumulation zone affected by compressional ridges and long wavelengths anticlines of the BBMS1 (Figs. 11, 12). These anticlines are NW-SE striking folds likely covered by recent deposits (Figs. 14, 15) while, to the NW, fold hinges of BBMS1 show higher amplitude and strike toward WNW-ESE (hinges 1–8 red in Fig. 12). These observations suggest a prevailing BBMS1 sense of movement toward the SSW, perpendicular to the strike of the high amplitude fold's hinges (Fig. 12).

The different sense of translation of the MTDs and the geometry of the BBMS1 detachment with a ramp toward the SW, suggest that the chaotic sediments represent a Mass Transport Deposit Complex (MTDC) with the more recent BBMS1 deforming the older BBMS. Considering fold geometry and restoring to horizontal the deformation, we reconstruct undeformed lengths of the MTDC of ~29 km along Line-A (Fig.

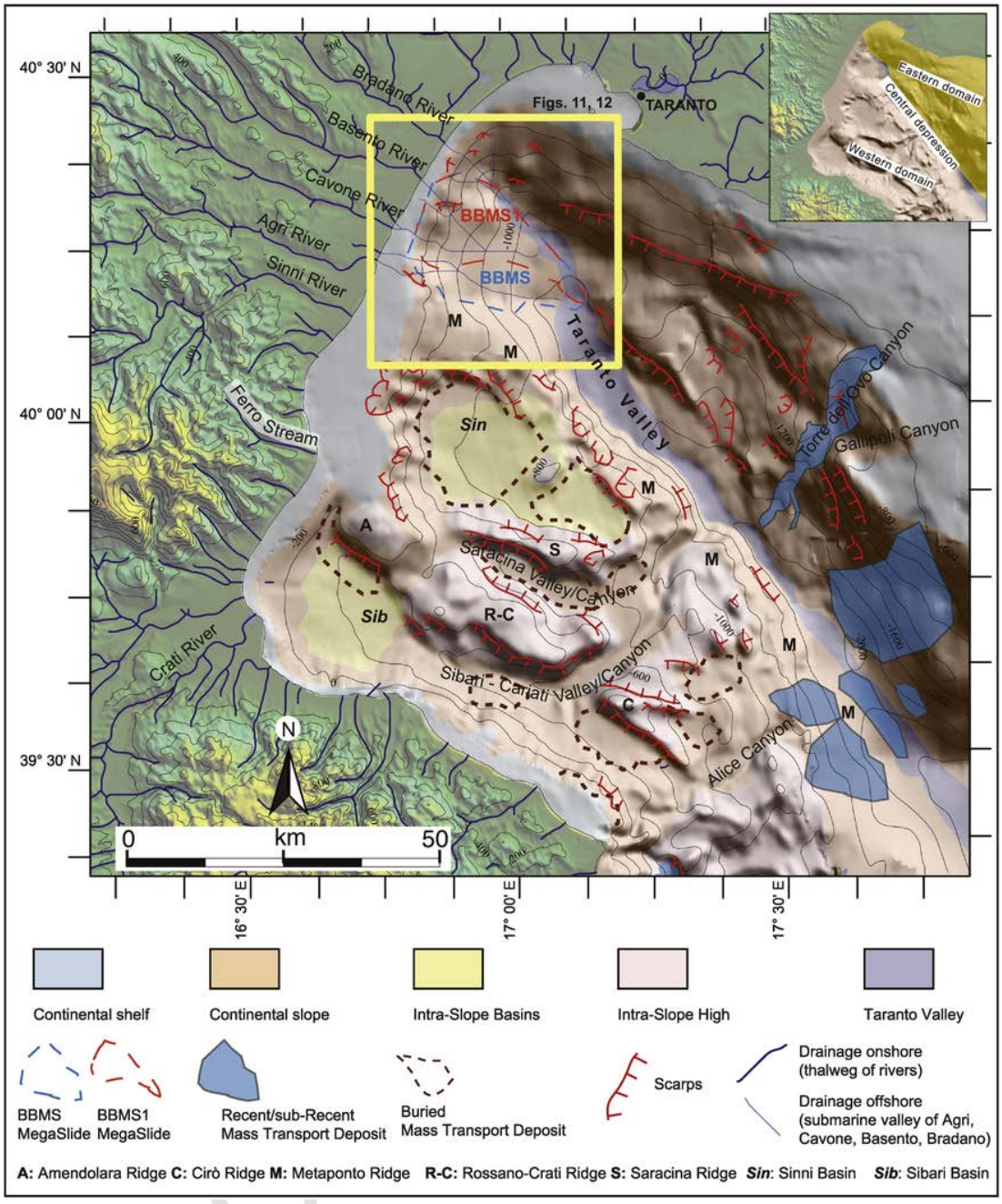

Fig. 10. Gulf of Taranto morpho-bathymetry (data from GMRT database; see Table 1). Drainage network built with Globalmapper Analysis tool - Generate Watershed. Morphological domains are modified after (Rossi et al., 1989). Three morpho-structural domains have been defined (see inset at the top right corner): western domain, central depression, eastern domain. The central depression coincides with the Taranto Submarine Valley. The yellow box indicates the area with a steeper continental slope near the head of the submarine Taranto Valley where the BBMS (blue dashed line) and BBMS1 (red dashed line) were identified through analysis of seismic data (see also Fig. 11). These reliefs are divides between submarine valleys which are aligned with the direction of the onshore Agri, Cavone, Basento, Bradano rivers; these submarine valleys are also tributaries of the Taranto Valley. The latter represents the basin plain nowadays. The Taranto valley and its submarine tributaries might replicate the valleys incised during the LGM sea level low-stand. (See text for details.) (For interpretation of the references to colour in this figure legend, the reader is referred to the web version of this article.)

13a) and ~15 km along Line-B (Fig. 13b) that allow to assess the overall run-out distances for the BBMS and BBMS1 in between ~700 m (shortening along Line A) and ~200 m (shortening along Line B). A minimum run-out distance can also be estimated measuring the displacement along the side walls scarps (extensional faults) in Line-A, Line-B and line F75-89A + B (Figs. 13a, b, 14a). In the depth-converted model (Suppl. mat. 2), these extensional faults have a cumulative throw of about 100 m. Thus, the run-out distance of the MTDC should lay between 100 m (minimum – extensional faults cumulative displacement) and 700 m (maximum – unfolded folds).

Concluding, the MTDs are constituted by middle-late Pleistocene clay-rich deposits that have glided in part toward the SE (BBMS) and in part toward the SSW (BBMS1) above the basal detachment that has a modelled slope of ~3° toward the SE (Fig. 15) with a run out distance between 100 m and 700 m.

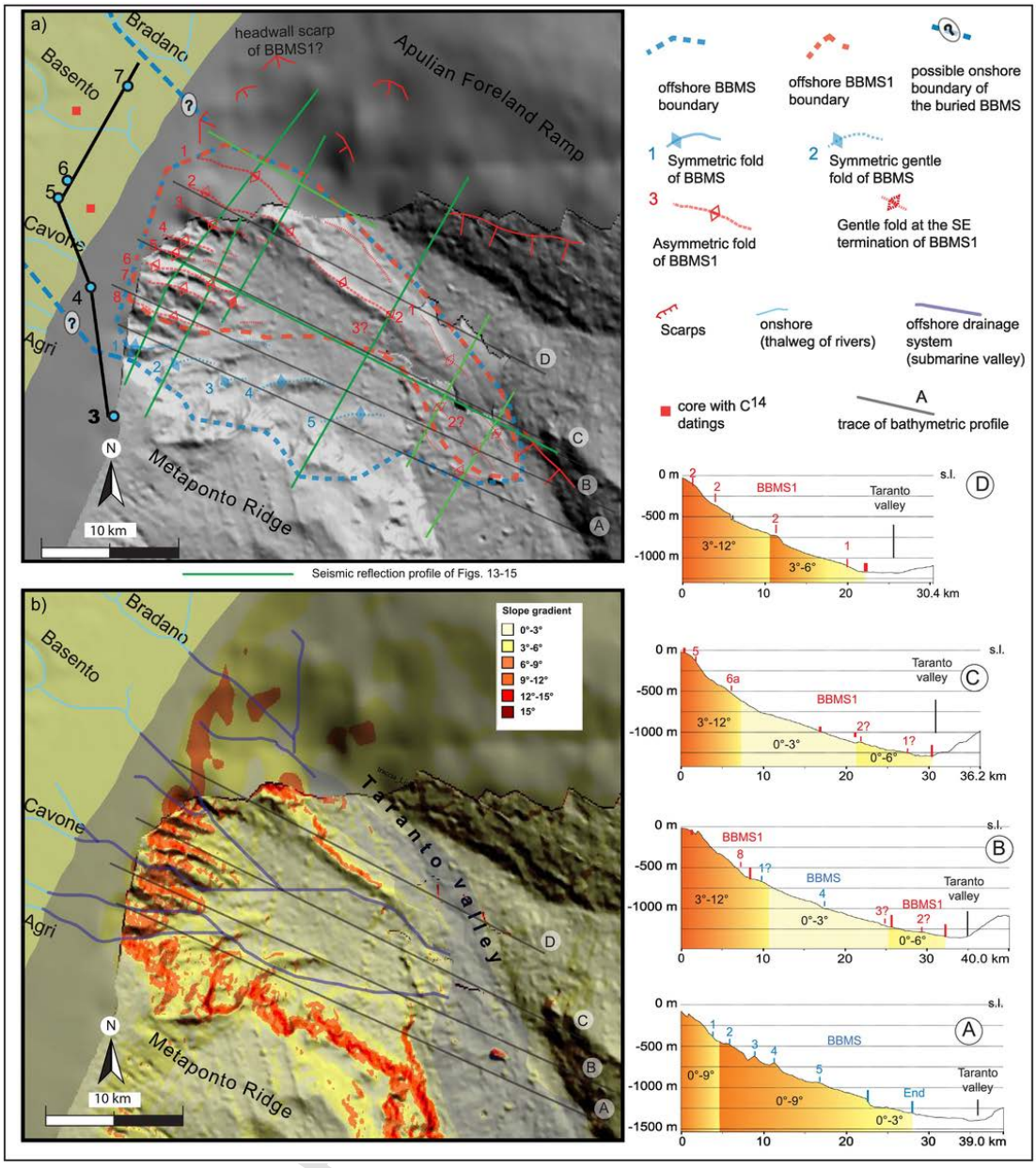

Fig. 11. a) Bathymetry and b) slope gradient map associated with bathymetric profiles (A, B, C, D) showing the differences of the seafloor characteristics in different sectors of the BBMS and BBMS1. In a) and b), note the correspondence between the relief and the folds of the BBMS and BBMS1 as observed in seismic reflection profiles (see Fig. 13–15). Also note that the relief controls the submarine drainage system. See text for details. The bathymetry is from https://www.seadatanet.org/ and Italian Navy Hydrographic Office (see Table 1).

5.3. The MTDC and the structural setting

Comparison of morphostructural maps with distribution and internal geometries of the MTDC suggests a strong interplay between structural setting, uplift processes and the emplacement of the MTDC. Geometry and internal structures show that the MTD complex is aligned parallel to the Taranto Valley. BBMS appears to move subparallel to the Apenninic front while BBMS1 moves downslope from the downflexing Apulian Foreland Ramp (Fig. 12). Such complex structural framework produces mass wasting in the two directions, and funnels re-sedimented deposits to the center of the Bradano foredeep to form the MTDC (Fig. 12).

Since the MTDC maximum length is aligned with the outermost thrust front of the Southern Apennines (Metaponto Ridge), mass wasting processes are controlled by the pre-existing topography. The basal gliding surface of the BBMS is located, in fact, above the Metaponto ridge and slip along the bounding thrusts makes the NE limb of Metaponto ridge steeper, enhancing mass movements. Similarly, the gliding surface of the BBMS1 is above and parallel to the Apulian Foreland Ramp (Figs. 8, 9) (see Section 4.2) which progressively downflexes toward the SW and increases the steepness of the slope enhancing the remobilization processes.

6. Discussion

The newly described BBMS-BBMS1 deposits integrate the archive of MTDs in the Calabrian Arc and Gulf of Taranto areas (Ceramicola et al., 2014; Meo et al., 2016; Rebesco et al., 2009; Zecchin et al., 2018). Structures and geometries of the MTDC suggest that internal deformation varies along its length with high sediment disruption and deformation in the NW region (Figs. 13–14), relatively no deformation in

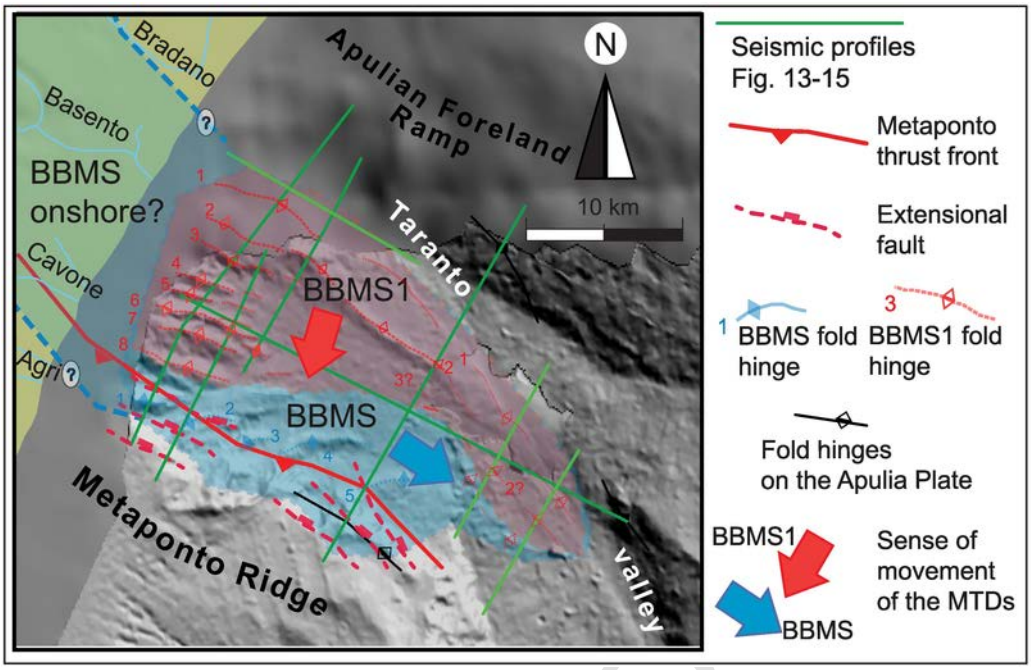

Fig. 12. Map of BBMS-BBMS1 as reconstructed and their sense of movements. The main tectonic structures of Fig. 7 are reported together with the fold hinges observed on the bathymetry and seismic reflection profiles (see Figs. 13–15). See text for details. The bathymetry is from https://www.seadatanet.org/ and Italian Navy Hydrographic Office (see Table 1).

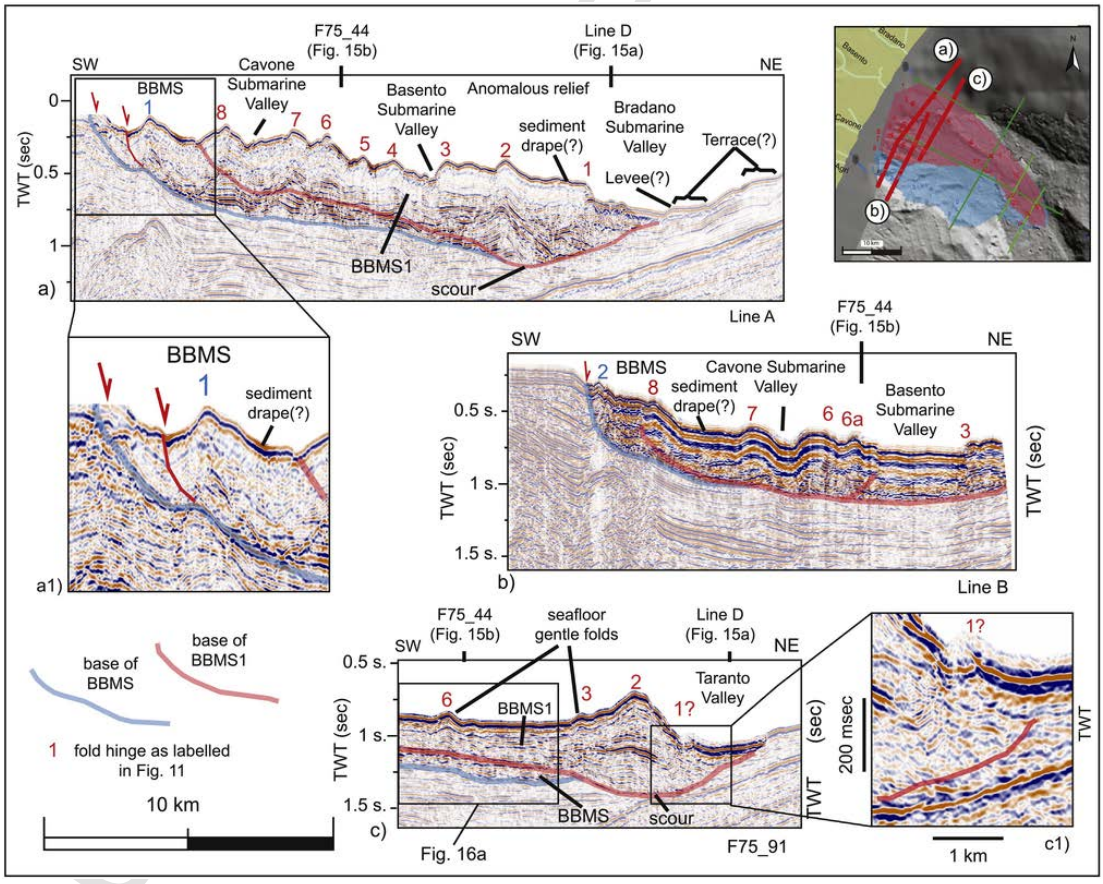

Fig. 13. a, b, c) NE-SW seismic profiles across the northwestern and more deformed portion of the BBMS-BBMS1. The pre-sliding units are white shaded. In a) chaotic and deformed reflections at the SW edge of BBMS. In c), chaotic seismic facies beneath Taranto Valley belongs to the BBMS1 (see enlarged square of c1). Chaotic seismic facies cutting the underlaying plane parallel reflectors mark the base of BBMS while a high amplitude reflector marks the base of BBMS1 (see Fig. 16a). For the location of the seismic profiles see inset and Figs. 4, 11.

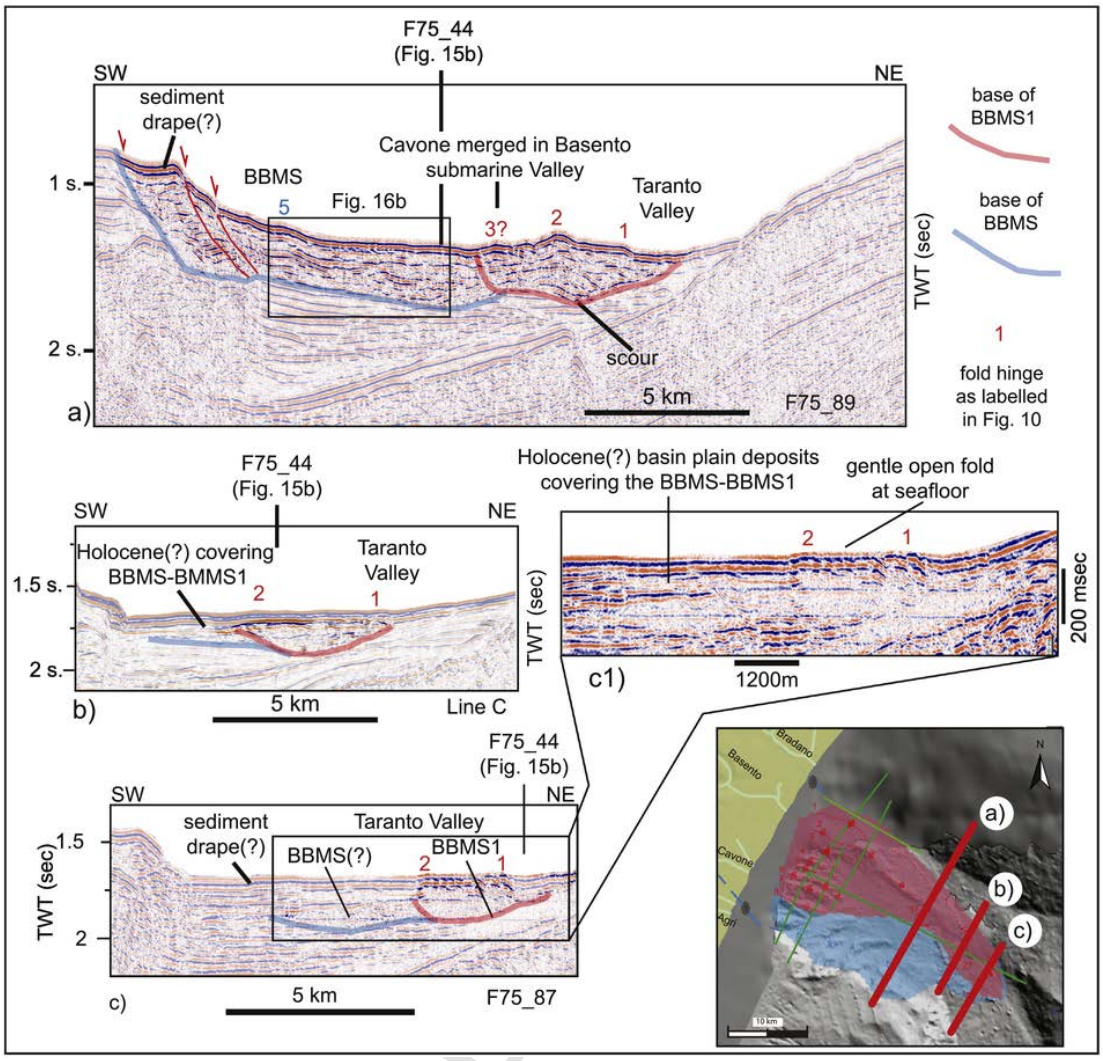

Fig. 14. a, b, c) Detail NE-SW seismic profiles across the southeastern and less deformed portion of the BBMS-BBMS1. Note that the BBMS covered by Holocene(?) basin plain deposit filling the Taranto Valley. Note also the gentle open folds that deforms the seafloor; they are associated to the BBMS1 (see enlarged rectangle in c1). The pre-sliding units are white shaded. For the location see inset and Figs. 4, 11.

the central part (Fig. 15) and slight sediment deformation close to its SE termination (Figs. 14, 15). The gliding mass is associated with side-walls scarps corresponding to extensional faults affecting the NW-most portion of the Metaponto Ridge. The gliding mass appears displaced toward the sea in a direction sub-parallel (BBMS) and perpendicular (BBMS1) to the Apennines front (Fig. 12). The BBMS-BBMS1 have a modelled basal detachment that shows a regular and concave upward geometry which contrasts with the highly ragged and folded top surface. The sliding masses, constituted by clay-rich deposits (Fig. 17), had an overall movement along the maximum dip (~3° toward SE) of the basal detachment and are internally deformed by at least 13 anticlines reaching the seafloor. Eight of these anticlines are related to the translation of the younger BBMS1 toward SSW. The SE termination of the BBMS-BBSM1 appears to be locally covered by about 0.11 sec TWT (about 120 m) of stratified slope-to-basin plain deposits of the Taranto Valley (Fig. 14) that are most likely Holocene fine-grained turbidites (Falco et al., 2016b). To the NW, at the head of the Taranto submarine Valley, Holocene sediments might drape the BBMS-BBMS1 but they are not clearly imaged on seismic profiles.

Although it is not possible to determine whether BBMS1 overprinted or triggered deformations within an earlier BBMS, its position, geometry, internal deformations and detachment suggest it post-dates the BBMS. In our interpretation, the gentle open folds at the SE termination of BBMS1 (Fig. 11) can be considered folds formed at the accumulation zone of the BBMS and later remobilized and refolded by the emplacement of BBMS1. Furthermore, the basal detachment of the BBMS1 ramps upward within the BBMS suggesting that the BBMS1 occurred when the BBMS was already emplaced (Figs. 13–15, Suppl. mat. 1). An alternative interpretation suggests that the more external fold belonging to the BBMS1 represents the frontal anticline ramp of the Southern Apennines (Teofilo et al., 2018). However, this interpretation is incompatible with the observed concave upward detachment surface that dips to the SE representing the gliding surface of the MTDC. Thus, the MTDC does not belong to the accretionary complex of the subduction system, but rather represents mass wasting processes in the foredeep. BBMS and BBMS1, in fact, have seismic characteristic and size estimates in agreement with a slope-attached Mass Transport Complex (Moscardelli and Wood, 2008) similar to other MTDs in the area (Ceramicola et al., 2014). On the other hand, the maximum estimated length/width ratio L/W = 2.53 (Fig. 18c) would imply that the BBMS-BBMS1 is a detached-MTD sensu Moscardelli and Wood (2008, 2015). The L/W estimated values for BBMS-BBMS1 reinforce the hypothesis that available data allow only partial mapping of the complex, and that it most likely extends onshore toward the NW. In fact, applying the

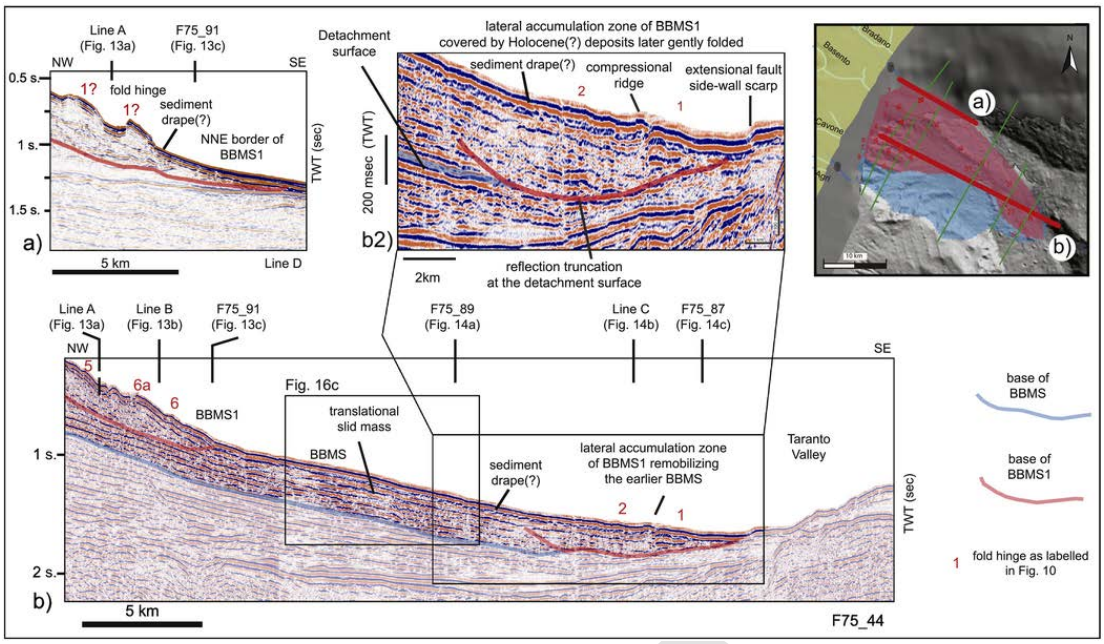

Fig. 15. a, b) Details NW-SE seismic reflection profiles crossing the BBMS-BBMS1. The more deformed sector is in the NW portion and belongs to the BBMS1. Most of the BBMS is a translational slid mass and it appears undeformed. The pre-sliding units are white shaded and the detachment surface at the top of the pre-sliding units (see Fig. 16c). For the locations see inset and Figs. 4, 11.

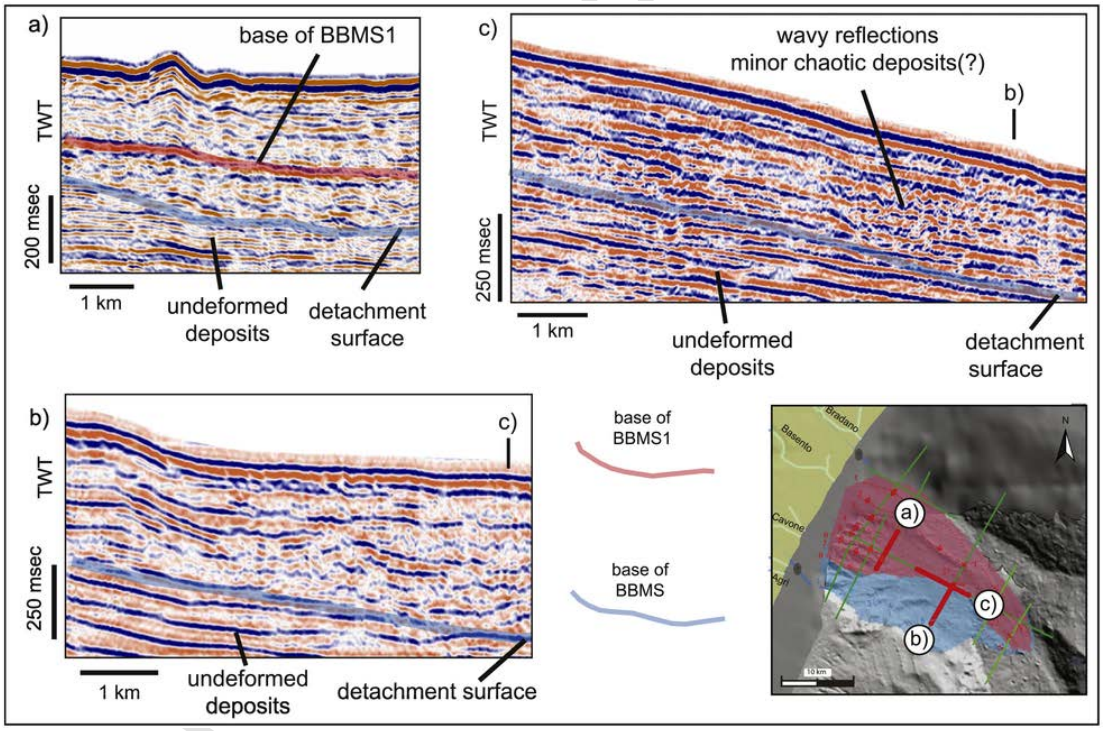

Fig. 16. Details of the detachment surface of BBMS-BBMS1 along a) seismic profile F75_91, b) seismic profile F75_44 and c) seismic profiles F75_44. The BBMS is characterized by discontinuous, partly transparent and deformed reflections (a, b) while it appears undeformed in its central portion where it is mainly a translational slid mass (c). Underneath the detachment, the pre-sliding units are characterized by laterally continuous reflections (a, b, c). The BBMS1 is more deformed internally and a strong high amplitude reflector locally marks the base of BBMS1 above the BBMS (a). For the locations see inset map and Figs. 4, 11.

MTD classification of Moscardelli and Wood (2008, 2015), the measured width of ~20 km for the BBMS-BBMS1 implies a minimum of 80 km in longitudinal extension thus longer than the estimated 57 km. However, the dimensions reconstructed through the analyses of seismic data are similar to the recently studied onshore-offshore Crotone Megalandslide (Zecchin et al., 2018).

Several parameters, including variable internal geometries and run-out distances (100 to 700 m) and the occurrence of at least one re-activation episode (BBMS1), suggest that the new MTDC in the Gulf of Taranto is a composite mega-slide formed during at least two failure events displacing, mobilizing and deforming shelfal and slope deposits along the same basal detachment. The geometry of the composite

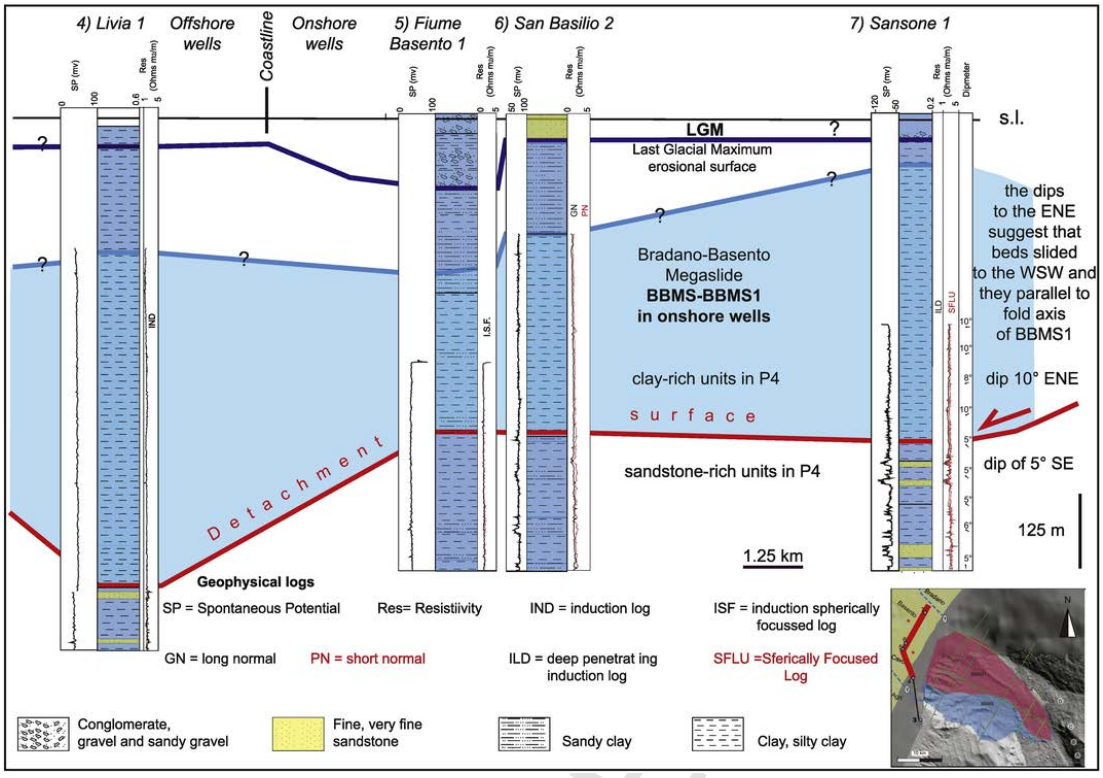

Fig. 17. Logs of onshore wells (Sansone 1, San Basilio 2, Fiume Basento 1) and one offsohre well (Livia 1) with details of the lithological and electrical properties (spontaneous potential and resistivity). The lithological variations, the petrophysical properties and the changes in dip-meter measurements are used to constrain the detachment surface of the BBMS and BBMS1. The top surface of the BBMS and BBMS1 cannot be defined but it is likely covered by Holocene deposits. See text for details.

mega-slide and its internal characters (nearly undeformed slided masses), pose the question if the BBMS-BBMS1 is the result of a mass wasting event, either single of multiple, or if it is related to gravitational tectonics. The latter is common in both convergent and extensional margins (de Vera et al., 2010; Espurt et al., 2018; Murray et al., 2018; Pettinga, 2004; Scarselli et al., 2016; Wang et al., 2017; Winkelmann et al., 2010) and it is invoked for the orogeny collapse (Espurt et al., 2018; Rey et al., 2001; Tibaldi and Bonali, 2018). Gravitational tectonics may generate remobilized deposits with low internal deformation and may reach size of tens of kilometers. If fluids circulation occurs, these gravity-driven deposits might be preferentially associated with sediment's creeping (Hsu et al., 2018; Li et al., 2016; Mountjoy et al., 2014; Thöle et al., 2016). However, undeformed regions within Mass Transport Deposits are common (Gafeira et al., 2010) and available data do not allow to fully discriminate between the two different processes (i.e. mass wasting deposits and gravitational tectonics deposits). The portion of the BBMS–BBMS1 closest to the coast appears as wasted masses of sediments, whereas, the deeper portion of the BBMS-BBMS1 appears as a slide which did not suffer a huge amount of transport (700 m maximum). The limited number of chaotic deposits and the observed mild folding of continuous sediment layers are in favor of gravitational deformations in the SE termination of the MTDC. We cannot exclude that in the more distal part of our MTDC, inclination of the submarine slope might have favored gravitational tectonics associated with subsurface sediments creeping.

While detection of incipient or ancient gravity deposits from interpretation of high resolution seafloor morphology and/or seismic reflection profiles is relatively straightforward, age determinations and triggering mechanisms of MTD is not trivial. In the next sections, we will attempt to estimate the range of ages for the BBMS-BBMS1 emplacement and to discuss evidence for possible triggering mechanisms and geo-hazards.

6.1. Age of MTDs emplacement

Well-logs and seismic stratigraphic correlations suggest that the BBMS-BBMS1 represents one of the latest depositional events within the youngest tectono-sedimentary cycle P4 made of middle-late Pleistocene shelf-slope deposits resting above the Middle Pleistocene Unconformity (MPSU) (Zecchin et al., 2015) (Fig. 6). BBMS and BBMS1 show a morphological expression at the seafloor, although the SE termination of BBMS is locally covered by Holocene fine-grained deposits (Fig. 14), whose distribution has been constrained in the Gulf of Taranto offshore (Falco et al., 2016b). On the other hand, if the BBMS-BBMS1 reach onshore up to the Metaponto region (Fig. 18), they are also covered by alluvial deposits (Fig. 17). In the offshore, there are no age determinations for deposits immediately capping the MTDs, except for few cores in Holocene deposits collected in the Taranto Valley (Falco et al., 2016a, 2016b). Onshore, two C^{14} ages of 11.853 ± 60 yr BP (mollusk fragment) and 13.075 ± 90 yr BP (plant fragment) were determined on samples collected from the Metaponto alluvial plain-shelfal deposits (Tropeano et al., 2013). The two samples were collected at a depth of ~58 m b.s.l., within a 30–100 m thick aggrading-prograding wedge of shelf and alluvial plain sediments overlaying a subaerial erosion surface. This erosion surface cuts through fine-grained shelf-to-slope facies and is correlated to the LGM (Bentivenga et al., 2004; Caputo et al., 2010; Tropeano et al., 2013), i.e., between 19.000 and 26.500 yr BP (Clark et al., 2009), or ~20,000 yr BP (Lambeck et al., 2014; Zecchin et al., 2016). Increased sedimentation rates of ~4.5 mm/year and a rapid burial of the LGM topography were reported after the LGM (Falco et al., 2016c; Tropeano et al., 2013). However, the thalwegs of present-day onshore rivers (Bradano, Basento, Agri and Cavone) closely correspond with the buried LGM incised valleys (Tropeano et al., 2013; Pieri, 2015). The correspondence

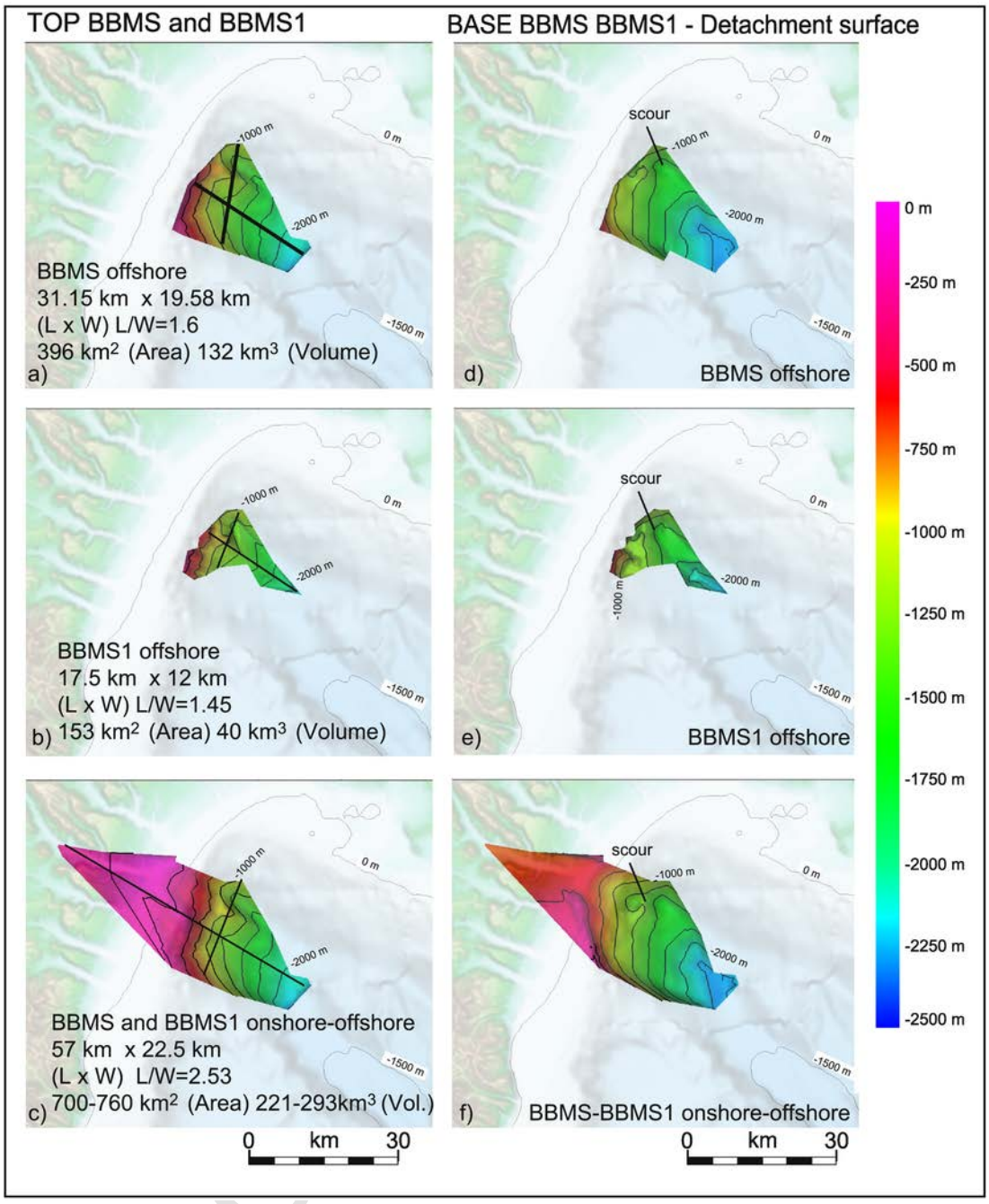

Fig. 18. Surfaces modelling of top and bottom (detachment) surfaces of BBMS and BBMS1. The surfaces are modelled based on time to depth converted seismic reflection profiles (see Suppl. mat. 2). The top- and bottom-surfaces of BBMS-BBMS1 derive from the Delaunay triangulation with sample density of 100 lines and the resampling Lines interval of 30 m and 1000 m. For details on the surface modelling refer to Appendix 1. a) Plane view of top of the offshore BBMS and b) BBMS1; c) the top surface of BBMS considering its possible onshore extension. d) Base of the BBMS offshore or detachment surface of the studied MTDC. e) Base of BBMS1. f) Base of BBMS including the possible onshore prosecution. The surfaces were modelled with the aid of software Move of Midland Valley.

between the present-day incisions and LGM river paths onshore should also be the case of the submarine drainage system (Figs. 10, 11). The limited width of the shelf and the presence of a deep incised valley, such as the Taranto Valley, both suggest that the shelf has been recently eroded (Section 5.1) and it might replicate the LGM incisions. In addition, we can also note that BBMS-BBMS1 morphologies control the positions of the Taranto Valley and its tributaries, the Bradano, Basento, Agri and Cavone submarine valleys (Figs. 10, 11). These tributaries also incise and create levees on top of BBMS1 (Fig. 13a). In this respect, the relief observed along the slope (Fig. 11) might be relict submarine morphological highs created by the MTDC. Therefore, the relief created by the MTDC might control both the incisions of the LGM erosional surface and the recent submarine drainage system. This submarine drainage system fed (during the LGM) and feed (at present) the Taranto Valley with terrigenous deposits that locally cap the BBMS (Fig. 15) and possibly the BBMS1 due to the uncertainties to clearly define the top surface of the MTDC. In absence of accurate dating and imaging for such deposits, we can assume that they post-date the LGM erosional surface and form meters thick sediment drape of the BBMS-BBMS1. The above observations and assumptions imply that the emplacement of the BBMS-BBMS1 should predate the LGM (late Pleistocene).

We also note that the southeastern termination of the MTDC shows gentle sediment folding reaching the seafloor (Figs. 11, 14c), suggesting possible recent (post-LGM) remobilization but the thickness of Holocene draping is below the resolution of seismic images in most of the seismic profiles (Figs. 13–15). Concluding, though the BBMS1 appears to be younger than the BBMS, their emplacement dates back to the LGM or very likely earlier and rough seafloor morphologies might suggest either a possible Holocene reactivation or relict morphologies.

6.2. Possible triggering mechanisms

Widespread emplacement of megaturbidites throughout the Mediterranean during the last glacial maximum was reported in the western Mediterranean Sea (Rothwell et al., 2000). Catastrophic destabilisation of the margins after a long period of accumulation with an increased rate of sediment supply was invoked as the main triggering mechanism for the deposition of the Balearic and Herodotus abyssal plain megabeds (Rothwell et al., 2000). However, LGM sea level low stand should not play a fundamental role in triggering the deposition of the study MTDs because their emplacement should pre-dates the erosional surface of the LGM (see Section 6.1); nonetheless, older sea level changes cannot be discharged as trigger for the emplacement of the MTDC. In this view, pre-LGM time sea level fall causing pore pressure variations within sediments may enhance slope instability and mass failures as well as fluid seepage. Up to now, evidence of fluid circulation associated with either past seepages or clathrates was never reported in the area. Then, fluid seepage and gas hydrate dissociation are unlikely triggering mechanisms.

The BBMS and BBMS1 are relatively recent features showing a close connection with tectonic structures being oriented parallel to the frontal thrust of the orogenic wedge, i.e., the Metaponto Ridge Frontal Thrust and Apulian Foreland Ramp (Fig. 7; Section 5.3). This occurrence has been described also in other regions (Strozyk et al., 2009; Zitter et al., 2012; Alves et al., 2013; Strasser et al., 2013; Moscardelli and Wood, 2015). For this reason, and because the study area is tectonically active with moderate to intense seismicity (Fig. 2), seismic shaking should be considered a likely triggering mechanism for sediment remobilization. A single earthquake can initiate slope instability and sediment re-mobilization, especially in confined basins characterized by high sedimentation rates and bordered by rapidly uplifting coastal mountains (Polonia et al., 2013, 2016b). Such earthquake triggering is also reported in oceanic areas such as the Japan trench, where the Mw 9.0 2011 Tohoku-Oki earthquake generated a slump 2–3 km wide and 13 km long (~27.7 km^2) affecting the entire trench (Strasser et al., 2013), and the Mw 7.2 1929 Grand Bank earthquake (Newfoundland, Canada) (Heezen and Ewing, 1952; Piper and Morrison, 1999). In the Japan case study, the bathymetry of the trench was completely modified by the earthquake event, due to the formation of extensional and contractional faults, the latter being shifted 2 km trench-ward. A striking Mediterranean example linking seismic shaking, giant slope failures and tsunami generation is the Mw 8.5 365 CE Crete earthquake and tsunami, which triggered the deposition of up to 20 m thick mega-turbidite on the basin floor of the eastern Mediterranean (Polonia et al., 2013) in area >150,000 km^2 (Polonia et al., 2017a) and for a total volume of at least 162 × 10 km^3 (Rebesco et al., 2000).

The possible link between BBMS-BBMS1 and a large magnitude earthquake should be tested with paleoseismological studies. However, most paleoseismological studies were carried out onshore, and rarely constrain late Pleistocene or older earthquake events. Only recently, a paleosesimological study revealed that the Cittanova fault has been the source of one of the most catastrophic earthquakes in Europe (the 5th February 1783 M_w 7 earthquake of Cittanova fault in the Calabrian Arc) and caused slip events dated back between 13,080–12,970 yr BP and 12,935–12,681 yr BP (Galli and Peronace, 2015). Precise dating of sediments draping the BBMS-BBMS1 might allow the establishment of a correlation between the study MTDC and these seismic events. Clear markers of recent tectonic activity were reported onland, such as folded marine terraces (Santoro et al., 2013; Ferranti et al., 2014), extensional faults (Galli and Bosi, 2002; Galli and Peronace, 2015) and transcurrent faults (Galli et al., 2008) which were active since middle Pleistocene to present-day. A single earthquake, a cluster of earthquakes or a phase of intensified tectonic activity at the Metaponto Ridge or at deeper fault-related folds of the Apulia plate (Figs. 7–9), might thus be considered a possible triggering mechanism for BBMS-BBMS1 emplacement. Since it is difficult to identify a specific earthquake among those already known in the area (Galli et al., 2008), the BBMS-BBMS1, as well as other older MTDs in the Gulf of Taranto area, might indicate that at geological time scales, the record of earthquake might be incomplete. This hypothesis calls for a more detailed study of the sedimentary record in the Bradano Foredeep basin to define age and the recurrence time of resedimented deposits.

Seismic data show that portions of the BBMS-BBMS1 maintain their original sedimentary layering and mild or no deformations, and this indicates that gravitational tectonics might be the mechanism that forms the MTDC. The gravitational instabilities and sediment remobilization might be related to both the relatively high uplift rate of the Calabrian Arc and the downflexing Apulian plate in the last 1 Ma (Billi et al., 2011; Doglioni et al., 1994; Faccenna et al., 2014). If gravitational tectonics is considered to have driven the deposition of the BBMS-BBMS1, their emplacement should not be synchronous with any major earthquakes. Again, detailed paleoseismological studies are mandatory to better discriminate seismically triggered slope failures versus gravitational tectonics. In both reconstructions, mapping MTDs has important implications for geo-hazard assessment in coastal areas.

6.3. Implications for geo-hazards

The emplacement of MTDC (BBMS-BBMS1) due to gravitational tectonics, sediment creeping not associated to sudden fault ruptures would imply slow motion and deformation of the moving masses not able to generate an instantaneous seafloor rise capable to generate a tsunami. In this scenario, sediment creeping might represent also a recent process due to local accommodations above the MTDs (Fig. 11) enhancing shallow sliding of thin sediment packages as already recognized in Calabrian margin (Ceramicola et al., 2014; Rebesco et al., 2009).

However, the emplacement of BBMS-BBMS1 possibly associated with paleo-earthquakes cannot be excluded for two main reasons: 1) the MTDC is one of the largest in the area (Fig. 18), despite its onland portion is not well constrained yet; 2) both onland and offshore tectonic structures are active since middle Pleistocene and presumably associated with paleo-earthquakes (Ferranti et al., 2014; Galli et al., 2008; Galli and Bosi, 2002; Santoro et al., 2013). If the BBMS-BBMS1 is considered as triggered by seismic shaking a different tsunami-hazard for the Gulf of Taranto needs to be evaluated. Seismically triggered submarine landslides are considered possible causes of tsunamis (Tappin, 2010) also if they are relatively small. Sliding volumes of 4–8 km^3 have been modelled and reported to be possible causes of tsunamis in association with seafloor co-seismic ruptures (Satake, 2012). The Taranto submarine landslide, with an estimated volume of 0.30 km^3 (10 to 100 times smaller than the MTDs in this work), has been modelled and results suggest that it generated a tsunami wave up to 1.75 m height along the coast (Meo et al., 2016). According to historical catalogues (Ambraseys, 1962; Tinti et al., 2004; Maramai et al., 2014), tsunami hazard along the Ionian Sea coast is high. Tsunami hazard assessment has necessarily to include also far-field sources in the Mediterranean (Papadopoulos et al., 2014; Polonia et al., 2016b). The effects of historical tsunamis are reported both along the Ionian

coast of Calabria and, to a lesser degree, along the Adriatic coast of Puglia, where, pre-historical and historical tsunami deposits were detected (Mastronuzzi and Sansò, 2000; Mastronuzzi et al., 2007; Milia et al., 2017). Despite the difficulties in distinguishing local tsunamis from storm layers in the geological records (Dawson and Stewart, 2007; Bourgeois, 2009; Engel and Brückner, 2011), faunal mixtures derived from different near-shore paleoenvironments are indicative of tsunami waves (Peters and Jaffe, 2010; Engel and Brückner, 2011; Smedile et al., 2011). Recent detailed stratigraphic work on middle to late Pleistocene deposits carried out onshore along the Gulf of Taranto coasts did not reveal high-energy facies that could possibly be related to tsunamis (Amorosi et al., 2014; Capraro et al., 2017). However, these stratigraphic studies are local, and focus on detailed sea-level fluctuations and global scale stratigraphic correlations. More studies need to be done in order to exclude tsunamis deposits in the Pleistocene-Holocene sedimentary record onshore the Gulf of Taranto. In this respect, the present work could provide useful insights to modelling and guide the search for onshore/offshore, direct/indirect proxies about possible tsunami wave/s generated by BBMS and BBMS1 emplacement in pre-LGM time or younger remobilization events.

.

7. Summary and conclusion

In the Gulf of Taranto, large-size Mass Transport Deposits, named the "Bradano Basento Mega Slide" (BBMS) and a younger slide mass (BBMS1), were identified and mapped. They form the largest MTD complex described in the offshore Gulf of Taranto. The BBMS shows an area of ~396 km^2, a volume of 130 km^3 while the younger BBMS1 shows an area of ~153 km^2 and a volume of ~40 km^3; the run-out distances are up to few hundreds of meters. These estimates are conservative, since BBMS and BBMS1 might have an onshore buried extension, not imaged by our marine data. The BBMS and BBMS1 affected and eroded the topmost portion of the outer Southern Apennines front, and transported toward the SE and SSW middle-late Pleistocene clay/silty-clay deposits.

Several lines of evidence, including that the BBMS-BBMS1 gliding surface appears to be controlled by main tectonic structures in the area, suggest that the most likely triggering mechanism for the emplacement of the MTDs is seismic activity. For this reason, the BBMS and BBMS1 might be considered paleo-seismological markers of large magnitude earthquakes in the Bradano Foredeep basin. Based on stratigraphic correlations, carried out using well-logs and the ages of correlative deposits onshore, the age of the MTDs is late Pleistocene and predates the LGM; though younger remobilization events cannot be excluded. The analysis of MTDs has thus the potential to reconstruct seismic activity back in time. The offshore paleo-seismological markers will complete the onshore paleo-seismological record and will contribute to better clarify the seismic behavior of this geologically complex region. On the other hand, because portions of BBMS and BBMS1 show undeformed seismic facies or mild deformations at their offshore termination, it cannot be excluded that the studied MTDC is related to gravitational tectonics and sediment creeping decreasing the tsunami hazard in the study region.

Nonetheless, the size and the distribution of the Mass Transport Deposits in the sedimentary record of the Bradano Foredeep emphasize the need to re-evaluate and to better appraise the potential for large earthquakes and tsunamis along the densely populated coast of the Gulf of Taranto that is also site of industrial infrastructures.

Acknowledgements

The work funded by PRIN 2010–11 Project "Active and recent geodynamics of Calabrian Arc and accretionary complex in the Ionian Sea" (Scientific Resp. L. Torelli). We thank ENI S.p.A. for allowing us to have access to their data and providing the permission to publish the seismic images; in particular, thanks to A. L. Cazzola, A. Fattorini and C. Cattaneo. Thanks to Italian Navy Hydrographic Office for providing bathymetric map. We are grateful to Celine Grall, Loredana Moscardelli and an anonymous reviewer for their comments and useful suggestions that greatly improved the early versions of the paper. In particular, we are indebted to Celine Grall for her careful and insightful reviews that greatly improved the manuscript.

Appendix A. Supplementary data

Supplementary data to this article can be found online at https://doi.org/10.1016/j.margeo.2018.11.008.

References

Álvarez-Gómez, J.A., Aniel-Quiroga, , González, M., Olabarrieta, M., Carreño, E., 2011. Scenarios for earthquake-generated tsunamis on a complex tectonic area of diffuse deformation and low velocity: the Alboran Sea, Western Mediterranean. Mar. Geol. 284, 55–73. https://doi.org/10.1016/j.margeo.2011.03.008.

Alves, T.M., Strasser, M., Moore, G.F., 2013. Erosional features as indicators of thrust fault activity (Nankai Trough, Japan). Mar. Geol. 356, 5–18. https://doi.org/10.1016/j.margeo.2013.07.011.

Ambraseys, N.N., 1962. Data for the investigation of the seismic sea-waves in the Eastern Mediterranean. Bull. Seismol. Soc. Am. 52, 895–913.

Amorosi, A., Antonioli, F., Bertini, A., Marabini, S., Mastronuzzi, G., Montagna, P., Negri, A., Rossi, V., Scarponi, D., Taviani, M., Angeletti, L., Piva, A., Vai, G.B., 2014. The Middle-Upper Pleistocene Fronte Section (Taranto, Italy): an exceptionally preserved marine record of the Last Interglacial. Glob. Planet. Chang. 119, 23–38. https://doi.org/10.1016/j.gloplacha.2014.04.007.

Bentivenga, M., Coltorti, M., Prosser, G., Tavarnelli, E., 2004. A new interpretation of terraces in the Taranto Gulf: the role of extensional faulting. Geomorphology 60, 383–402. https://doi.org/10.1016/j.geomorph.2003.10.002.

Bigi, G., Bonardi, G., Catalano, R., Cosentino, D., Lentini, F., Parotto, M., Sartori, R., Scandone, P., Turco, E., 1990. Structural Model of Italy Scale 1:500.000, Sheets 4–6. In: Bigi, G., Cosentino, D., Parotto, M., Sartori, R., Scandone, P. (Eds.), Progetto Finalizzato Geodinamica - Sottoprogetto: Modello Strutturale Tridimensionale. CNR-Consiglio Nazionale delle Ricerche, Roma.

Billi, A., Faccenna, C., Bellier, O., Minelli, L., Neri, G., Piromallo, C., Presti, D., Scrocca, D., Serpelloni, E., 2011. Recent tectonic reorganization of the Nubia-Eurasia convergent boundary heading for the closure of the western Mediterranean. Bull. Soc. Geol. Fr. 182, 279–303. https://doi.org/10.2113/gssgfbull.182.4.279.

Bohannon, R.G., Gardner, J.V., 2004. Submarine landslides of San Pedro Escarpment, southwest of Long Beach, California. Mar. Geol. 203, 261–268. https://doi.org/10.1016/S0025-3227(03)00309-8.

Bonardi, G., Cavazza, W., Perrone, V., Rossi, S., 2001. Calabria-Peloritani terrane and northern Ionian Sea. In: Vai, G.B., Martini, I.P. (Eds.), Anatomy of an Orogen: The Apennines and Adjacent Mediterranean Basins. Springer Netherlands, Dordrecht, pp. 287–306. https://doi.org/10.1007/978-94-015-9829-3_17.

Bortoluzzi, G., Polonia, A., Torelli, L., Arton, A., Carlini, M., Carone, S., Carrara, G., Cuffaro, M., Del Bianco, F., D'Oriano, F., Ferrante, V., Gasperini, L., Ivaldi, R., Terra, La, Amedeo, A., Ligi, M., Locritani, M., Muccini, F., Mussoni, P., Priore, F., Riminucci, F., Romano, S., Stanghellini, G., Artoni, A., Carlini, M., Carone, S., Carrara, G., Cuffaro, M., Del Bianco, F., D'Oriano, F., Ferrante, V., Gasperini, L., Ivaldi, R., Laterra, A., Ligi, M., Locritani, M., Muccini, F., Mussoni, P., Priore, F., Riminucci, F., Romano, S., Stanghellini, G., 2017. Styles and rates of deformation in the frontal accretionary wedge of the Calabrian Arc (Ionian Sea): controls exerted by the structure of the lower African plate. Ital. J. Geosci. 136, 347–364. https://doi.org/10.3301/IJG.2016.11.

Bourgeois, J., 2009. In: Robinson, A.R., Bernard, E.N. (Eds.), Geologic Effects and Records of Tsunamis. Harvard University Press, The Sea, pp. 53–91.

Brown, H.E., Holbrook, W.S., Hornbach, M.J., Nealon, J., 2006. Slide structure and role of gas hydrate at the northern boundary of the Storegga Slide, offshore Norway. Mar. Geol. 229, 179–186. https://doi.org/10.1016/j.margeo.2006.03.011.

Butler, R.W.H., 2009. Relationships between the Apennine thrust belt, foredeep and foreland revealed by marine seismic data, offshore Calabria. Ital. J. Geosci. 128, 269–278. https://doi.org/10.3301/IJG.2009.128.2.269.

Capozzi, R., Artoni, A., Torelli, L., Lorenzini, S., Oppo, D., Mussoni, P., Polonia, A., 2012. Neogene to Quaternary tectonics and mud diapirism in the Gulf of Squillace (Crotone-Spartivento Basin, Calabrian Arc, Italy). Mar. Pet. Geol. 35, 219–234. https://doi.org/10.1016/j.marpetgeo.2012.01.007.

Capraro, L., Ferretti, P., Macrì, P., Scarponi, D., Tateo, F., Fornaciari, E., Bellini, G., Dalan, G., 2017. The Valle di Manche section (Calabria, Southern Italy): a high resolution record of the Early-Middle Pleistocene transition (MIS 21-MIS 19) in the Central Mediterranean. Quat. Sci. Rev. 165, 31–48. https://doi.org/10.1016/j.quascirev.2017.04.003.

Caputo, R., Bianca, M., D'Onofrio, R., 2010. Ionian marine terraces of southern Italy: insights into the Quaternary tectonic evolution of the area. Tectonics 29, https://doi.org/10.1029/2009TC002625, (n/a-n/a).

Carbone, S., Senatore, M.R., Pescatore, T.S., 2013. Foglio. 523, 1–162.

Catalano, R., Doglioni, C., Merlini, S., 2001. On the Mesozoic Ionian Basin. Geophys. J. Int. 144, 49–64. https://doi.org/10.1046/j.0956-540X.2000.01287.x.

Ceramicola, S., Praeg, D., Coste, M., Forlin, E., Cova, A., Colizza, E., Critelli, S., 2014. Submarine Mass Movements and Their Consequences, Advances in Natural and Technological Hazards Research. Springer International Publishing, Cham, https://doi.org/10.1007/978-3-319-00972-8.

Clark, P.U., Dyke, A.S., Shakun, J.D., Carlson, A.E., Clark, J., Wohlfarth, B., Mitrovica, J.X., Hostetler, S.W., McCabe, A.M., 2009. The Last Glacial Maximum. Science (80-.) 325, 710–714. https://doi.org/10.1126/science.1172873.

Cohen, J.K., Stockwell, J.W., 2010. CWP/SU: Seismic Un*x release no. 42: an open source software package for seismic research and processing. In: Cent. Wave Phenomena, Color. Sch. Mines.

Craig Shipp, R., Weimer, P., Posamentier, H.W., 2011. In: SEPM. (Ed.), Mass-Transport Deposits in Deepwater Settings. 96, SEPM Spec. Publ, Tulsa, Oklahoma.

Dawson, A.G., Stewart, I., 2007. Tsunami deposits in the geological record. Sediment. Geol. 200, 166–183. https://doi.org/10.1016/j.sedgeo.2007.01.002.

de Vera, J., Granado, P., McClay, K., 2010. Structural evolution of the Orange Basin gravity-driven system, offshore Namibia. Mar. Pet. Geol. 27, 223–237. https://doi.org/10.1016/j.marpetgeo.2009.02.003.

del Ben, A., Barnaba, C., Taboga, A., 2008. Strike-slip systems as the main tectonic features in the Plio-Quaternary kinematics of the Calabrian Arc. Mar. Geophys. Res. 29, 1–12. https://doi.org/10.1007/s11001-007-9041-6.

DISS Working Group, 2015. Database of Individual Seismogenic Sources (DISS), Version 3.2.0: A Compilation of Potential Sources for Earthquakes Larger Than M 5.5 in Italy and Surrounding Areas. https://doi.org/10.6092/INGV.IT-DISS3.2.0, (www document).

Doglioni, C., Mongelli, F., Pieri, P., Pieri, P., 1994. The Puglia uplift (SE Italy): an anomaly in the foreland of the Apenninic subduction due to buckling of a thick continental lithosphere. Tectonics 13, 1309–1321. https://doi.org/10.1029/94TC01501.

Doglioni, C., Merlini, S., Cantarella, G., 1999. Foredeep geometries at the front of the Apennines in the Ionian Sea (central Mediterranean). Earth Planet. Sci. Lett. 168, 243–254. https://doi.org/10.1016/S0012-821X(99)00059-X.

Engel, M., Brückner, H., 2011. The identification of palaeo-tsunami deposits – a major challenge in coastal sedimentary research. Coastline Rep. 17, 65–80.

Eruteya, O.E., Safadi, M., Waldmann, N., Makovsky, Y., Ben-Avraham, Z., 2016. Seismic geomorphology of the Israel Slump Complex in the Levant Basin (SE Mediterranean). In: Lamarche, G., Mountjoy, J., Bull, S., Hubble, T., Krastel, S., Lane, E., Micallef, A., Moscardelli, L., Mueller, C., Pecher, I., Woelz, S. (Eds.), Submarine Mass Movements and Their Consequences, Advances in Natural and Technological Hazards Research. Springer International Publishing, Cham, pp. 39–47. https://doi.org/10.1007/978-3-319-20979-1_4.

Espurt, N., Brusset, S., Baby, P., Henry, P., Vega, M., Calderon, Y., Ramirez, L., Saillard, M., 2018. Deciphering the Late Cretaceous-Cenozoic structural evolution of the North Peruvian Forearc System. Tectonics 37, 251–282. https://doi.org/10.1002/2017TC004536.

Faccenna, C., Becker, T.W., Miller, M.S., Serpelloni, E., Willett, S.D., 2014. Isostasy, dynamic topography, and the elevation of the Apennines of Italy. Earth Planet. Sci. Lett. 407, 163–174. https://doi.org/10.1016/j.epsl.2014.09.027.

Falco, M., Meo, A., Amore, F.O., Senatore, M.R., 2016. A multi-disciplinary approach of sediment-core from the Taranto continental slope (Northern Ionian Sea). First results. Rend. Online Soc. Geol. Ital. 41, 39.

Falco, M., Meo, A., Ercilla, G., Alonso, B., Senatore, M.R., 2016. High resolution stratigraphic and sedimentological analysis on a deep-water gravity core: Taranto Canyon (Northern Ionian Sea) case history. Rend. Online Soc. Geol. Ital. 41, 40.

Falco, M., Meo, A., Ercilla, G., Alonso, B., Senatore, M.R., 2016. Centennial-scale climatic variability in the Gulf of Taranto during the upper Holocene. Rend. Online Soc. Geol. Ital. 41, 38. https://doi.org/10.3301/IJG.2011.09.

Ferranti, L., Burrato, P., Pepe, F., Santoro, E., Mazzella, M.E., Morelli, D., Passaro, S., Vannucci, G., 2014. An active oblique-contractional belt at the transition between the Southern Apennines and Calabrian Arc: the Amendolara Ridge, Ionian Sea, Italy. Tectonics 33, 2169–2194. https://doi.org/10.1002/2014TC003624.

Festa, A., Dilek, Y., Gawlick, H.-J., Missoni, S., 2014. Mass-transport deposits, olistostromes and soft-sediment deformation in modern and ancient continental margins, and associated natural hazards. Mar. Geol. 356, 1–4. https://doi.org/10.1016/j.margeo.2014.09.001.

Gafeira, J., Long, D., Scrutton, R., Evans, D., 2010. 3D seismic evidence of internal structure within Tampen Slide deposits on the North Sea Fan: are chaotic deposits that chaotic?. J. Geol. Soc. Lond. 167, 605–616. https://doi.org/10.1144/0016-76492009-047.

Galli, P., Bosi, V., 2002. Paleoseismology along the Cittanova fault: implications for seismotectonics and earthquake recurrence in Calabria (southern Italy). J. Geophys. Res. 107, 2044. https://doi.org/10.1029/2001JB000234.

Galli, P.A.C., Peronace, E., 2015. Low slip rates and multimillennial return times for M w 7 earthquake faults in southern Calabria (Italy). Geophys. Res. Lett. 42, 5258–5265. https://doi.org/10.1002/2015GL064062.

Galli, P., Galadini, F., Pantosti, D., 2008. Twenty years of paleoseismology in Italy. Earth Sci. Rev. 88, 89–117. https://doi.org/10.1016/j.earscirev.2008.01.001.

Gibbard, P.L., Head, M.J., Walker, M.J.C., 2010. Formal ratification of the Quaternary System/Period and the Pleistocene Series/Epoch with a base at 2.58 Ma. J. Quat. Sci. 25, 96–102. https://doi.org/10.1002/jqs.1338.

Grall, C., Henry, P., Westbrook, G.K., Çağatay, M.N., Thomas, Y., Marsset, B., Borschneck, D., Saritas, H., Cifçi, G., Géli, L., 2014. Mass Transport Deposits Periodicity Related to Glacial Cycles and Marine-Lacustrine Transitions on a Ponded Basin of the Sea of Marmara (Turkey) Over the Last 500 ka. 595–603. https://doi.org/10.1007/978-3-319-00972-8_53.

Gueguen, E., Doglioni, C., Fernandez, M., 1998. On the post-25 Ma geodynamic evolution of the western Mediterranean. Tectonophysics 298, 259–269. https://doi.org/10.1016/S0040-1951(98)00189-9.

Guidoboni, E., Ferrari, G., Mariotti, D., Comastri, A., Tarabusi, G., Valensise, G., 2015. Catalogue of strong earthquakes in Italy 461 B.C.–1997 and Mediterranean area 760 B.C.–1500. Ist. Naz. di Geofis. e Vulcanol. In: http://storing.ingv.it/cfti4med/, (www document).

Heezen, B.C., Ewing, W.M., 1952. Turbidity currents and submarine slumps, and the 1929 Grand Banks [Newfoundland] earthquake. Am. J. Sci. 250, 849–873. https://doi.org/10.2475/ajs.250.12.849.

Hsu, S.-K., Lin, S.-S., Wang, S.-Y., Tsai, C.-H., Doo, W.-B., Chen, S.-C., Lin, J.-Y., Yeh, Y.-C., Wang, H.-F., Su, C.-W., 2018. Seabed gas emissions and submarine landslides off SW Taiwan. Terr. Atmos. Ocean. Sci. 29, 7–15. https://doi.org/10.3319/TAO.2016.10.04.01.

ISIDe working Group, 2016. Italian seismological instrumental and parametric database: http://iside.rm.ingv.it/iside/standard/index.jsp and http://cnt.rm.ingv.it/ [www document]. In: Ist. Naz. di Geofis. e Vulcanol. https://doi.org/10.13127/ISIDe.

Jolivet, L., Faccenna, C., 2000. Mediterranean extension and the Africa-Eurasia collision. Tectonics 19, 1095–1106. https://doi.org/10.1029/2000TC900018.

Katz, O., Reuven, E., Aharonov, E., 2015. Submarine landslides and fault scarps along the eastern Mediterranean Israeli continental-slope. Mar. Geol. 369, 100–115. https://doi.org/10.1016/j.margeo.2015.08.006.

Kawamura, K., Laberg, J.S., Kanamatsu, T., 2014. Potential tsunamigenic submarine landslides in active margins. Mar. Geol. 356, 44–49. https://doi.org/10.1016/j.margeo.2014.03.007.

Lambeck, K., Rouby, H., Purcell, A., Sun, Y., Sambridge, M., 2014. Sea level and global ice volumes from the Last Glacial Maximum to the Holocene. Proc. Natl. Acad. Sci. 111, 15296–15303. https://doi.org/10.1073/pnas.1411762111.

Li, W., Alves, T.M., Wu, S., Rebesco, M., Zhao, F., Mi, L., Ma, B., 2016. A giant, submarine creep zone as a precursor of large-scale slope instability offshore the Dongsha Islands (South China Sea). Earth Planet. Sci. Lett. 451, 272–284. https://doi.org/10.1016/j.epsl.2016.07.007.

Lo Iacono, C., Gràcia, E., Zaniboni, F., Pagnoni, G., Tinti, S., Bartolomé, R., Masson, D.G., Wynn, R.B., Lourenccedil, N., de Abreu, M.P., Dañobeitia, J.J., Zitellini, N., 2012. Large, deepwater slope failures: implications for landslide-generated tsunamis. Geology 40, 931–934. https://doi.org/10.1130/G33446.1.

Locati, M., Rovida, A., Albini, P., Stucchi, M., 2014. The AHEAD portal: a gateway to European historical earthquake data. Seismol. Res. Lett. 85, 727–734. https://doi.org/10.1785/0220130113.

Locati, M., Camassi, R., Rovida, A., Ercolani, E., Bernardini, F., Castelli, V., Caracciolo, C.H., Tertulliani, A., Rossi, A., Azzaro, R., D'Amico, S., Conte, S., Rocchetti, E., 2016. DBMI15, the 2015 version of the Italian macroseismic database. [www document]. In: Ist. Naz. di Geofis. e Vulcanol. https://doi.org/10.6092/INGV.IT-DBMI15.

Malinverno, A., Ryan, W.B.F., 1986. Extension in the Tyrrhenian Sea and shortening in the Apennines as result of arc migration driven by sinking of the lithosphere. Tectonics 5, 227–245. https://doi.org/10.1029/TC005i002p00227.

Maramai, A., Brizuela, B., Graziani, L., 2014. The Euro-Mediterranean tsunami catalogue. Ann. Geophys. https://doi.org/10.4401/ag-6437.

Martín-Merino, G., Fernández, L.P., Colmenero, J.R., Bahamonde, J.R., 2014. Mass-transport deposits in a Variscan wedge-top foreland basin (Pisuerga area, Cantabrian Zone, NW Spain). Mar. Geol. 356, 71–87. https://doi.org/10.1016/j.margeo.2014.01.012.

Maslin, M., Mikkelsen, N., Vilela, C., Haq, B., 1998. Sea-level – and gas-hydrate–controlled catastrophic sediment failures of the Amazon Fan. Geology 26, 1107. https://doi.org/10.1130/0091-7613(1998)026<1107:SLAGHC>2.3.CO;2.

Mastronuzzi, G., Sansò, P., 2000. Boulders transport by catastrophic waves along the Ionian coast of Apulia (southern Italy). Mar. Geol. 170, 93–103. https://doi.org/10.1016/S0025-3227(00)00068-2.

Mastronuzzi, G., Pignatelli, C., Sansò, P., Selleri, G., 2007. Boulder accumulations produced by the 20th of February, 1743 tsunami along the coast of southeastern Salento (Apulia region, Italy). Mar. Geol. 242, 191–205. https://doi.org/10.1016/j.margeo.2006.10.025.

McAdoo, B.G., Watts, P., 2004. Tsunami hazard from submarine landslides on the Oregon continental slope. Mar. Geol. 203, 235–245. https://doi.org/10.1016/S0025-3227(03)00307-4.

Meo, A., Falco, M., Chiocci, F.L., Senatore, M.R., 2016. Kinematics and the tsunamigenic potential of Taranto Landslide (northeastern Ionian Sea): morphological analysis and modeling. In: Aversa, S., Cascini, L., Picarelli, L., Scavia, C. (Eds.), Landslides and Engineered Slopes. Experience, Theory and Practice. Taylor and Francis Inc., pp. 1409–1416. https://doi.org/10.1201/b21520-173.

Milia, A., Iannace, P., Torrente, M.M., 2017. Active tectonic structures and submarine landslides offshore southern Apulia (Italy): a new scenario for the 1743 earthquake and subsequent tsunami. Geo-Mar. Lett. 1–11. https://doi.org/10.1007/s00367-017-0493-7.

Moscardelli, L., Wood, L., 2008. New classification system for mass transport complexes in offshore Trinidad. Basin Res. 20, 73–98. https://doi.org/10.1111/j.1365-2117.2007.00340.x.

Moscardelli, L., Wood, L., 2015. Morphometry of mass-transport deposits as a predictive tool. Geol. Soc. Am. Bull. 128, B31221.1. https://doi.org/10.1130/B31221.1.

Mostardini, F., Merlini, S., 1986. Appennino centro-meridionale. Sezioni geologiche e proposta di modello strutturale. Mem. Soc. Geol. Ital. 35, 59.

Mountjoy, J.J., Pecher, I., Henrys, S., Crutchley, G., Barnes, P.M., Plaza-Faverola, A., 2014. Shallow methane hydrate system controls ongoing, downslope sediment transport in a low-velocity active submarine landslide complex, Hikurangi Margin, New Zealand. Geochem. Geophys. Geosyst. 15, 4137–4156. https://doi.org/10.1002/2014GC005379.

Murray, J.B., van Wyk de Vries, B., Pitty, A., Sargent, P., Wooller, L., 2018. Gravitational sliding of the Mt. Etna massif along a sloping basement. Bull. Volcanol. 80, 40. https://doi.org/10.1007/s00445-018-1209-1.

Murty, T.S., 2003. Tsunami wave height dependence on landslide volume. Pure Appl. Geophys. 160, 2147–2153. https://doi.org/10.1007/s00024-003-2423-z.

Palano, M., Ferranti, L., Monaco, C., Mattia, M., Aloisi, M., Bruno, V., Cannavò, F., Siligato, G., 2012. GPS velocity and strain fields in Sicily and southern Calabria, Italy: updated geodetic constraints on tectonic block interaction in the central Mediterranean. J. Geophys. Res. 117, B07401https://doi.org/10.1029/2012JB009254.

Papadopoulos, G.a., Gràcia, E., Urgeles, R., Sallares, V., De Martini, P.M., Pantosti, D., González, M., Yalciner, A.C., Mascle, J., Sakellariou, D., Salamon, A., Tinti, S., Karastathis, V., Fokaefs, A., Camerlenghi, A., Novikova, T., Papageorgiou, A., 2014. Historical and pre-historical tsunamis in the Mediterranean and its connected seas: geological signatures, generation mechanisms and coastal impacts. Mar. Geol. 354, 81–109. https://doi.org/10.1016/j.margeo.2014.04.014.

Patacca, E., Scandone, P., 2004. The Plio-Pleistocene Thrust Belt - Foredeep System in the Southern Apennines and Sicily (Italy). Boll. Soc. Geol. Ital. Spec. Vo. 93–129.

Pescatore, T., Senatore, M.R., 1986. A comparison between a present-day (Taranto Gulf) and a Miocene (Irpinian Basin) foredeep of the Southern Apennines (Italy). In: Allen, P.A., Homewood, P. (Eds.), Foreland Basins. Blackwell Publishing Ltd., Oxford, UK, pp. 169–182. https://doi.org/10.1002/9781444303810.ch8.

Peters, R., Jaffe, B., 2010. Identification of Tsunami Deposits in the Geologic Record; Developing Criteria Using Recent Tsunami Deposits. US Geol. Surv. Open File Rep.(43 pp).

Pettinga, J.R., 2004. Three-stage massive gravitational collapse of the emergent imbricate frontal wedge, Hikurangi subduction zone, New Zealand. N. Z. J. Geol. Geophys. 47, 399–414. https://doi.org/10.1080/00288306.2004.9515066.

Pieri, P., 2015. F. 508 Policoro. Carta Geologica d'Italia alla scala 1:50.000. ISPRA-Servizio Geologico d'Italia, Regione Basilicata, Roma.

Piper, D.J.W., Morrison, M.L., 1999. The sequence of events around the epicentre of the 1929 GrandBanks earthquake: initiation of debris flows and turbidity current inferred from sidescan sonar. Sedimentology 46, 79–97.

Polonia, A., Torelli, L., Mussoni, P., Gasperini, L., Artoni, A., Klaeschen, D., 2011. The Calabrian Arc subduction complex in the Ionian Sea: regional architecture, active deformation, and seismic hazard. Tectonics 30, TC5018https://doi.org/10.1029/2010TC002821.

Polonia, A., Bonatti, E., Camerlenghi, A., Lucchi, R.G., Panieri, G., Gasperini, L., 2013. Mediterranean megaturbidite triggered by the AD 365 Crete earthquake and tsunami. Sci. Rep. 3, 1285. https://doi.org/10.1038/srep01285.

Polonia, A., Torelli, L., Artoni, A., Carlini, M., Faccenna, C., Ferranti, L., Gasperini, L., Govers, R., Klaeschen, D., Monaco, C., Neri, G., Nijholt, N., Orecchio, B., Wortel, R., 2016. The Ionian and Alfeo–Etna fault zones: new segments of an evolving plate boundary in the central Mediterranean Sea?. Tectonophysics 675, 69–90. https://doi.org/10.1016/j.tecto.2016.03.016.

Polonia, A., Vaiani, S.C., de Lange, G.J., 2016. Did the A.D. 365 Crete earthquake/tsunami trigger synchronous giant turbidity currents in the Mediterranean Sea?. Geology 44, 191–194. https://doi.org/10.1130/G37486.1.

Polonia, A., Nelson, C.H., Romano, S., Vaiani, S.C., Colizza, E., Gasparotto, G., Gasperini, L., 2017. A depositional model for seismo-turbidites in confined basins based on Ionian Sea deposits. Mar. Geol. 384, 177–198. https://doi.org/10.1016/j.margeo.2016.05.010.

Polonia, A., Torelli, L., Gasperini, L., Cocchi, L., Muccini, F., Bonatti, E., Hensen, C., Schmidt, M., Romano, S., Artoni, A., Carlini, M., 2017. Lower plate serpentinite diapirism in the Calabrian Arc subduction complex. Nat. Commun. 8, 2172. https://doi.org/10.1038/s41467-017-02273-x.

Rebesco, M., Vedova, B.D., Cernobori, L., Aloisi, G., 2000. Acoustic facies of Holocene megaturbidites in the Eastern Mediterranean. Sediment. Geol. 135, 65–74. https://doi.org/10.1016/S0037-0738(00)00063-4.

Rebesco, M., Neagu, R.C., Cuppari, A., Muto, F., Accettella, D., Dominici, R., Cova, A., Romano, C., Caburlotto, A., 2009. Morphobathymetric analysis and evidence of submarine mass movements in the western Gulf of Taranto (Calabria margin, Ionian Sea). Int. J. Earth Sci. 98, 791–805. https://doi.org/10.1007/s00531-009-0429-1.

Reilinger, R., McClusky, S., 2011. Nubia-Arabia-Eurasia plate motions and the dynamics of Mediterranean and Middle East tectonics. Geophys. J. Int. 186, 971–979. https://doi.org/10.1111/j.1365-246X.2011.05133.x.

Reitz, M.a., Seeber, L., 2012. Arc-parallel strain in a short rollback-subduction system: the structural evolution of the Crotone basin (northeastern Calabria, southern Italy). Tectonics 31, 1–23. https://doi.org/10.1029/2011TC003031.

Rey, P., Vanderhaeghe, O., Teyssier, C., 2001. Gravitational collapse of continental crust: definitions, regimes, mechanisms and modes. Tectonophysics 342, 435–449.

Ricchetti, G., Ciaranfi, N., Luperto Sinni, E., Mongelli, F., Pieri, P., 1988. Geodinamica ed evoluzione sedimentaria e tettonica dell'avampaese apulo. Mem. Soc. Geol. Ital. 41, 57–82.

Rossetti, F., Goffé, B., Monié, P., Faccenna, C., Vignaroli, G., 2004. Alpine orogenic P-T-t-deformation history of the Catena Costiera area and surrounding regions (Calabrian Arc, southern Italy): the nappe edifice of north Calabria revised with insights on the Tyrrhenian-Apennine system formation. Tectonics 23, TC6011. https://doi.org/10.1029/2003TC001560.

Rossi, S., Auroux, C.C., Mascle, J., 1983. The Gulf of Taranto (Southern Italy): seismic stratigraphy and shallow structure. Mar. Geol. 51, 327–346. https://doi.org/10.1016/0025-3227(83)90110-X.

Rossi, S., Pescatore, T., Senatore, M.R., 1989. A geomorphological map of the Gulf of Taranto (southern Italy). Mar. Geol. 87, 103–104.

Rothwell, R.G., Thomson, J., Kähler, G., 1998. Low-sea-level emplacement of a very large Late Pleistocene "megaturbidite" in the western Mediterranean Sea. Nature 392, 377–380. https://doi.org/10.1038/32871.

Rothwell, R.G., Reeder, M.S., Anastasakis, G., Stow, D.A.V., Thomson, J., Kähler, G., 2000. Low sea-level stand emplacement of megaturbidites in the western and eastern Mediterranean Sea. Sediment. Geol. 135, 75–88. https://doi.org/10.1016/S0037-0738(00)00064-6.

Rouchy, J.M., Caruso, A., 2006. The Messinian salinity crisis in the Mediterranean basin: a reassessment of the data and an integrated scenario. Sediment. Geol. 188–189, 35–67. https://doi.org/10.1016/j.sedgeo.2006.02.005.

Roveri, M., Flecker, R., Krijgsman, W., Lofi, J., Lugli, S., Manzi, V., Sierro, F.J., Bertini, A., Camerlenghi, A., De Lange, G., Govers, R., Hilgen, F.J., Hübscher, C., Meijer, P.T., Stoica, M., 2014. The Messinian Salinity Crisis: past and future of a great challenge for marine sciences. Mar. Geol. 352, 25–58. https://doi.org/10.1016/j.margeo.2014.02.002.

Rovida, A., Camassi, R., Gasperini, P., Stucchi, M., 2011. CPTI11, the 2011 version of the Parametric Catalogue of Italian Earthquakes. Istituto Nazionale di Geofisica e Vulcanologia, Milano, Bologna, https://doi.org/10.6092/INGV.IT-CPTI11.

Ruh, J.B., 2016. Submarine landslides caused by seamounts entering accretionary wedge systems. Terra Nova 28, 163–170. https://doi.org/10.1111/ter.12204.

Ryan, W.B.F., Carbotte, S.M., Coplan, J.O., O'Hara, S., Melkonian, A., Arko, R., Weissel, R.A., Ferrini, V., Goodwillie, A., Nitsche, F., Bonczkowski, J., Zemsky, R., 2009. Global multi-resolution topography synthesis. Geochem. Geophys. Geosyst. 10, https://doi.org/10.1029/2008GC002332, (n/a-n/a).

Santoro, E., Ferranti, L., Burrato, P., Mazzella, M.E., Monaco, C., 2013. Deformed Pleistocene marine terraces along the Ionian Sea margin of southern Italy: unveiling blind fault-related folds contribution to coastal uplift. Tectonics 32, 737–762. https://doi.org/10.1002/tect.20036.

Satake, K., 2012. Tsunamis generated by submarine landslides. In: Yamada, Y., Kawamura, K., Ikehara, K., Ogawa, Y., Urgeles, R., Mosher, D., Chaytor, J., Strasser, M. (Eds.), Submarine Mass Movements and Their Consequences SE - 42, Advances in Natural and Technological Hazards Research. Springer, Netherlands, pp. 475–484. https://doi.org/10.1007/978-94-007-2162-3_42.

Scarselli, N., McClay, K., Elders, C., 2016. Seismic geomorphology of cretaceous megaslides offshore Namibia (Orange Basin): insights into segmentation and degradation of gravity-driven linked systems. Mar. Pet. Geol. 75, 151–180. https://doi.org/10.1016/j.marpetgeo.2016.03.012.

Schnyder, J.S.D., Eberli, G.P., Kirby, J.T., Shi, F., Tehranirad, B., Mulder, T., Ducassou, E., Hebbeln, D., Wintersteller, P., 2016. Tsunamis caused by submarine slope failures along western Great Bahama Bank. Sci. Rep. 6, 35925. https://doi.org/10.1038/srep35925.

Smedile, A., De Martini, P.M., Pantosti, D., Bellucci, L., Del Carlo, P., Gasperini, L., Pirrotta, C., Polonia, A., Boschi, E., 2011. Possible tsunami signatures from an integrated study in the Augusta Bay offshore (Eastern Sicily—Italy). Mar. Geol. 281, 1–13. https://doi.org/10.1016/j.margeo.2011.01.002.

Stockwell, J.W.J., 1997. Free Software in Education: A Case Study of CWP/SU: Seismic Un∗x. Lead. Edge, 1045–1049.

Stockwell, J.W., 1999. The CWP/SU: Seismic Un∗x package. Comput. Geosci. 25, 415–419. https://doi.org/10.1016/S0098-3004(98)00145-9.

Strasser, M., Kolling, M., Ferreira, C.D.S., Fink, H.G., Fujiwara, T., Henkel, S., Ikehara, K., Kanamatsu, T., Kawamura, K., Kodaira, S., Romer, M., Wefer, G., 2013. A slump in the trench: Tracking the impact of the 2011 Tohoku-Oki earthquake. Geology 41, 935–938. https://doi.org/10.1130/G34477.1.

Strozyk, F., Huhn, K., Strasser, M., Krastel, S., Kock, I., Kopf, A., 2009. New evidence for massive gravitational mass-transport deposits in the southern Cretan Sea, eastern Mediterranean. Mar. Geol. 263, 97–107. https://doi.org/10.1016/j.margeo.2009.04.002.

Tappin, D.R., 2010. Submarine mass failures as tsunami sources: their climate control. Philos. Trans. R. Soc. A Math. Phys. Eng. Sci. 368, 2417–2434. https://doi.org/10.1098/rsta.2010.0079.

Teofilo, G., Antoncecchi, I., Caputo, R., 2018. Neogene-Quaternary evolution of the offshore sector of the southern Apennines accretionary wedge, Gulf of Taranto, Italy. Tectonophysics https://doi.org/10.1016/j.tecto.2018.05.006, (#pagerange#).

Thöle, H., Kuhlmann, G., Lutz, R., Gaedicke, C., 2016. Late Cenozoic submarine slope failures in the southern North Sea - evolution and controlling factors. Mar. Pet. Geol. 75, 272–290. https://doi.org/10.1016/j.marpetgeo.2016.04.028.

Tibaldi, A., Bonali, F.L., 2018. Contemporary recent extension and compression in the central Andes. J. Struct. Geol. 107, 73–92. https://doi.org/10.1016/j.jsg.2017.12.004.

Tinti, S., Maramai, A., Graziani, L., 2004. The new catalogue of Italian Tsunamis. Nat. Hazards 33, 439–465. https://doi.org/10.1023/B:NHAZ.0000048469.51059.65.

Tropeano, M., Cilumbriello, A., Sabato, L., Gallicchio, S., Grippa, A., Longhitano, S.G., Bianca, M., Gallipoli, M.R., Mucciarelli, M., Spilotro, G., 2013. Surface and subsurface of the Metaponto Coastal Plain (Gulf of Taranto—southern Italy): Present-day- vs LGM-landscape. Geomorphology 203, 115–131. https://doi.org/10.1016/j.geomorph.2013.07.017.

Urgeles, R., Masson, D.G., Canals, M., Watts, A.B., Le Bas, T., 1999. Recurrent large-scale landsliding on the west flank of La Palma, Canary Islands. J. Geophys. Res. 104, 25331. https://doi.org/10.1029/1999JB900243.

Van Dijk, J.P., Bello, M., Brancaleoni, G.P., Cantarella, G., Costa, V., Frixa, A., Golfetto, F., Merlini, S., Riva, M., Torricelli, S., Toscano, C., Zerilli, A., 2000. A regional structural model for the northern sector of the Calabrian Arc (southern Italy). Tectonophysics 324, 267–320. https://doi.org/10.1016/S0040-1951(00)00139-6.

Volpi, V., Del Ben, A., Civile, D., Zgur, F., 2017. Neogene tectono-sedimentary interaction between the Calabrian Accretionary Wedge and the Apulian Foreland in the northern Ionian Sea. Mar. Pet. Geol. 83, 246–260. https://doi.org/10.1016/j.marpetgeo.2017.03.013.

Von Huene, R., Ranero, C.R., Watts, P., 2004. Tsunamigenic slope failure along the Middle America Trench in two tectonic settings. Mar. Geol. 203, 303–317. https://doi.org/10.1016/S0025-3227(03)00312-8.

Wang, X., Wang, Y., He, M., Chen, W., Zhuo, H., Gao, S., Wang, M., Zhou, J., 2017. Genesis and evolution of the mass transport deposits in the middle segment of the Pearl River canyon, South China Sea: insights from 3D seismic data. Mar. Pet. Geol. 88, 555–574. https://doi.org/10.1016/j.marpetgeo.2017.08.036.

Winkelmann, D., Geissler, W.H., Stein, R., Niessen, F., 2010. Post-megaslide slope stability north of Svalbard, Arctic Ocean. In: Mosher, D.C., Shipp, R.C., Moscardelli, L., Chaytor, Jason D., Baxter, Christopher D.P., Lee, Homa J., Urgeles, Roger (Eds.). Submarine Mass Movements and Their Consequences - 4th International Symposium. Springer, Dordrecht, pp. 279–287. https://doi.org/10.1007/978-90-481-3071-9_23.

Yamada, Y., Kawamura, K., Ikehara, K., Ogawa, Y., Urgeles, R., Mosher, D., Chaytor, J., Strasser, M., 2012. Submarine mass movements and their consequences. In: Yamada, Y., Kawamura, K., Ikehara, K., Ogawa, Y., Urgeles, R., Mosher, D., Chaytor, J., Strasser, M. (Eds.), Submarine Mass Movements and Their Consequences. Advances in Natural and Technological Hazards Research Springer Netherlands, Dordrecht, pp. 1–12. https://doi.org/10.1007/978-94-007-2162-3_1.

Zecchin, M., Nalin, R., Roda, C., 2004. Raised Pleistocene marine terraces of the Crotone peninsula (Calabria, southern Italy): facies analysis and organization of their deposits. Sediment. Geol. 172, 165–185. https://doi.org/10.1016/j.sedgeo.2004.08.003.

Zecchin, M., Civile, D., Caffau, M., Roda, C., 2009. Facies and cycle architecture of a Pleistocene marine terrace (Crotone, southern Italy): a sedimentary response to late Quaternary, high-frequency glacio-eustatic changes. Sediment. Geol. 216, 138–157. https://doi.org/10.1016/j.sedgeo.2009.03.004.

Zecchin, M., Civile, D., Caffau, M., Sturiale, G., Roda, C., 2011. Sequence stratigraphy in the context of rapid regional uplift and high-amplitude glacio-eustatic changes: the Pleistocene Cutro Terrace (Calabria, southern Italy). Sedimentology 58, 442–477. https://doi.org/10.1111/j.1365-3091.2010.01171.x.

Zecchin, M., Civile, D., Caffau, M., Muto, F., Di Stefano, A., Maniscalco, R., Critelli, S., 2013. The Messinian succession of the Crotone Basin (southern Italy) I: stratigraphic architecture reconstructed by seismic and well data. Mar. Pet. Geol. 48, 455–473. https://doi.org/10.1016/j.marpetgeo.2013.08.014.

Zecchin, M., Praeg, D., Ceramicola, S., Muto, F., 2015. Onshore to offshore correlation of regional unconformities in the Plio-Pleistocene sedimentary successions of the Calabrian Arc (central Mediterranean). Earth Sci. Rev. 142, 60–78. https://doi.org/10.1016/j.earscirev.2015.01.006.

Zecchin, M., Caffau, M., Ceramicola, S., 2016. Interplay between regional uplift and glacio-eustasy in the Crotone Basin (Calabria, southern Italy) since 0.45 Ma: a review. Glob. Planet. Chang. 143, 196–213. https://doi.org/10.1016/j.gloplacha.2016.06.013.

Zecchin, M., Accaino, F., Ceramicola, S., Civile, D., Critelli, S., Da Lio, C., Mangano, G., Prosser, G., Teatini, P., Tosi, L., 2018. The Crotone Megalandslide, southern Italy: architecture, timing and tectonic control. Sci. Rep. 8, 7778. https://doi.org/10.1038/s41598-018-26266-y.

Zitter, T.A.C., Grall, C., Henry, P., Özeren, M.S., Çağatay, M.N., Şengör, A.M.C., Gasperini, L., de Lépinay, B.M., Géli, L., 2012. Distribution, morphology and triggers of submarine mass wasting in the Sea of Marmara. Mar. Geol. 329–331, 58–74. https://doi.org/10.1016/j.margeo.2012.09.002.